Cognitive Neurodynamics (2025)19:85
https://doi.org/10.1007/s11571-025-10269-3

RESEARCH ARTICLE

Shap-driven explainable AI with simulated annealing for optimized seizure detection using multichannel EEG signal

Indu Dokare[1,2] · Sudha Gupta[1]

Received: 4 January 2025 / Revised: 8 April 2025 / Accepted: 29 April 2025

Abstract

The aim of this research is to combine Explainable AI (XAI) with advanced optimization techniques to provide a unique framework for seizure detection. This proposed work investigates how to enhance patient-specific and patient-non-specific seizure detection models by combining multiband feature extraction, SHAP-based feature selection, SMOTE, and a metaheuristic algorithm for hyperparameter tuning.The discrete wavelet transform (DWT) is used to decompose EEG signals to retrieve entropy-based and statistical information. Simulated Annealing (SA) is employed to optimize the Random Forest (RF) classifier's hyperparameters, and SHAP (SHapley Additive exPlanations) values are utilized for feature selection. Furthermore, a novel technique SHAP-RELFR has been demonstrated to select patient-non-specific features. Additionally, SMOTE is employed to handle imbalanced data. The proposed methodology is evaluated on the CHB-MIT and Siena datasets using both patient-specific and patient-non-specific feature selection approaches. Experimental findings demonstrate that the proposed methodology significantly improves the performance of seizure detection. The average accuracy, precision, sensitivity, specificity, F1-score, and AUC obtained for a patient-non-specific case are 96.58%, 95.19%, 94.52%, 98.02%, 94.72%, and 0.9452, respectively, using the CHB-MIT dataset. For the Seina dataset, the average accuracy, precision, sensitivity, specificity, F1-score, and AUC obtained for a patient-non-specific case are 94.81%, 94.51%, 94.04%, 96.87%, 94.28%, and 0.9400, respectively. Explainable AI combined with SMOTE and a metaheuristic optimization algorithm facilitates an enhanced seizure detection. The novel SHAP-RELFR method provides an effective patient-non-specific feature selection, enabling this approach to be applicable across diverse patients. This proposed framework offers a step toward enhancing clinical decision-making by providing interpretable and versatile seizure detection models.

Keywords Epilepsy · Multichannel EEG · Explainable artificial intelligence (XAI) · SHAP-RELFR · Simulated annealing · Random forest

Introduction

Millions of people worldwide suffer from epilepsy, a widespread neurological illness marked by repeated seizures that significantly compromise everyday functioning and pose health hazards (WHO 2022; Pais-Ribeiro and Meneses 2011; Narin 2022; Polat and Nour 2020). To reduce the hazards involved and improve the quality of life for those who have epilepsy, early seizure identification and treatment are essential (Amengual-Gual et al. 2019). Innovative methods for seizure detection have been made possible by advances in medical technology over time, with machine learning emerging as a promising avenue (Amengual-Gual et al. 2019). Electroencephalography

✉ Indu Dokare
indu.dokare@somaiya.edu

Sudha Gupta
sudhagupta@somaiya.edu

[1] Department of Electronics Engineering, K. J. Somaiya School of Engineering (formerly K. J. Somaiya College of Engineering), Somaiya Vidyavihar University, Vidyanagar, Vidyavihar East, Mumbai, Maharashtra 400077, India

[2] Department of Computer Engineering, Vivekanand Education Society's Institute of Technology, Chembur, Mumbai, Maharashtra 400074, India

Published online: 05 June 2025

(EEG) serves as a powerful non-invasive tool for diagnosing and analyzing various neurological (Siuly et al. 2016; Faust et al. 2008) and psychological conditions, including schizophrenia (Gupta et al. 2023, 2024), depressive disorders (Gupta et al. 2023; Bashir et al. 2023), mental state recognition (Yadav et al. 2023), and Parkinson's disease (Chandran and Perumalsamy 2018). Additionally, EEG plays a crucial role in applications such as brain-computer interfaces (BCI) (Ma et al. 2023; Malan and Sharma 2022; Kundu and Ari 2022), and drowsiness detection (Khare and Bajaj 2022), offering valuable insights into brain activity for both clinical and cognitive research. The ability of machine learning models, especially those trained on physiological signals like EEG recordings (Sanei and Chambers 2013), to detect seizure activity automatically has shown impressive potential (Sundaram et al. 1999). These models can offer precise and timely insights into the occurrence of seizures using the complex patterns (Amengual-Gual et al. 2019) and correlations found in the EEG data (Gotman and Gloor 1976). This allows for early intervention and the development of customized treatment strategies. A high-dimensional feature space with many features contributed by each channel is often generated by multichannel EEG signals. The sparser data and higher computational complexity in high-dimensional areas are referred to as the curse of dimensionality (Kondo et al. 2019). This may result in overfitting, degraded model performance, and an increase in the computing power needed for analysis (Cunningham 2008). However, there are significant challenges in accurate seizure detection due to the high dimensionality and complexity of multichannel EEG data.

To address these challenges, this research integrates sophisticated signal processing techniques, feature extraction strategies, and machine learning algorithms along with the SHAP value-based (Lundberg and Lee 2017; Hasan et al. 2023) feature selection method to develop a robust and interpretable seizure detection system. This proposed work has employed DWT along with statistical and entropy-based features. Finding the most useful features is essential to improve the model's performance and interpretability because of the high dimensionality of the extracted features. Further, the integration of SHAP values-based feature selection and SA optimized (Van Laarhoven 1987) RF classifier is demonstrated for seizure detection. The inherent lack of interpretability (Frasca et al. 2024) and explainability in the black-box models of machine learning algorithms makes automated seizure detection methods extremely difficult to adopt and accept in clinical practice (Frasca et al. 2024). Transparency and confidence in the decision-making process are essential for both patients and healthcare providers (Tallón-Ballesteros and Chen 2020), especially regarding health and well-being issues.

This research work seeks to highlight the role that SHAP values and SA-optimized RF classifiers (SA-RF) have played in developing the field of automated seizure detection and to show how they can have a transformative effect on the management of epilepsy through investigation. To summarize, the main contribution of this proposed work is as follows:

1. The integration of DWT with statistical and entropy-based features aids in capturing the complexity and distributional properties of the EEG signal.
2. Patient-specific feature selection based on SHAP values resulted in good interpretability of the machine learning model.
3. The class distribution is balanced by creating synthetic samples of the minority class using SMOTE.
4. SA-optimized RF classifier showed enhanced performance in distinguishing between seizure segments and non-seizure segments.
5. A novel method for patient-non-specific feature selection SHAP-RELFR has reported an excellent performance.

The next part of this paper is structured as follows: Sect. 2 reports the existing works. The detailed description of materials and methods is covered in Sect. 3, which includes the proposed approach, the datasets used, data preparation, filtering, segmentation, decomposition, feature extraction, feature selection, synthetic oversampling, and classifiers that are employed in this work. Experimental results and analysis are presented in Sect. 4. Additionally, the findings are compared with existing works, and a discussion of their implications is provided. Section 5 summarizes the key findings of the work and offers concluding remarks on the effectiveness of the proposed framework in EEG signal analysis for seizure detection.

Existing works

The relevant research on feature selection strategies, optimization techniques, and different methodologies employed in seizure detection is compiled in this section. Filter methods, a set of feature selection techniques, use parameters such as correlation coefficient and mutual information (Hassan et al. 2022; Hasan et al. 2022; Mostafiz et al. 2022) to rank features. These statistical metrics are used to assess each feature's importance apart from the machine learning algorithms in use. The correlation-based method (Mursalin et al. 2017), extended correlation-based (Guo et al. 2018), and correlation coefficients with distance correlation analysis (Ahmad et al. 2024) are a few feature selection methods that were employed for seizure detection. Wrapper methods are a kind of feature selection strategy where subsets of features are assessed according to

how well they work with a particular machine learning model. The wrapper feature subset selection method (Wijayanto et al. 2021), and recursive feature elimination (Wang and Lyu 2014; Hossain et al. 2024) are feature selection strategies that have been used to enhance the effectiveness of feature extraction. The work (Omidvar et al. 2021) has employed a genetic algorithm technique to pick more effective features, while the embedded methods, such as LASSO (Least Absolute Shrinkage and Selection Operator) (Peng et al. 2021) and tree-based methods using Gini importance (Sánchez-Hernández et al. 2022) were employed for feature selection in seizure detection.

Various optimization methods are employed for tuning the model's parameters in the field of machine learning. When perfect solutions to difficult combinatorial optimization problems are unfeasible (Macready and Wolpert 1996) or computationally prohibitive, a class of optimization methods known as metaheuristic algorithms is employed to address the problem effectively (Gandomi et al. 2013; Yang 2010). Metaheuristic algorithms frequently draw inspiration from physical processes, social behavior, or natural events (Gandomi et al. 2013). To iteratively enhance potential solutions, they also use notions like mutation, selection, and adaptation. The metaheuristic algorithms employed in seizure detection, such as genetic algorithm (GA) (Xiong et al. 2022) which is inspired by natural selection, show good performance. Particle swarm optimization (PSO) (Behnam and Pourghassem 2017; Yalcin et al. 2015) which is inspired by the social behavior of bird flocking, and ant colony optimization (ACO) (Behnam and Pourghassem 2015) which is inspired by the foraging behavior of ants, have also have been employed in seizure detection.

Many researchers have proposed different methods and models in the past for the detection of epilepsy using multichannel scalp EEG signals as shown in Fig. 1.

Every study reported here has utilized the CHB-MIT dataset for experimental purposes. The proposed work (Hassan et al. 2022) has employed DWT and statistical features along with mutual information score to select the best features. Min-max histogram approach for feature extraction was proposed (Yang et al. 2020) along with time domain and nonlinear features. Further, filter-embedded recursive feature elimination (RFE) was employed for feature selection along with SVM and XG Boost classifiers. The seizure detection proposed (Orosco et al. 2016) has employed a stationary wavelet transform, the spectral and energy features, and the statistical parameter Lambda of Wilks for feature selection. The study carried out (Behnam and Pourghassem 2017) has decomposed the EEG signal using uniform discrete Fourier transform (DFT), and the spectral features based on the DFT and discrete Walsh-Hadamard transform (DWHT) were extracted. To minimize the feature dimension, four statistical kernel-based techniques were separately employed. Particle swarm optimization (PSO) (Hossain et al. 2022) -probabilistic neural network (PNN) has been used as a feature selection and support vector machine (SVM) has been employed as a classifier. Frequency band-based feature selection using wavelet coefficients classified the EEG signal into seizure and non-seizure segments (Chen et al. 2017). A parse rational decomposition and Local Gabor Binary Pattern (LGBP) have been used to extract the features for seizure detection (Samiee et al. 2017). 1D LGBP features were computed for 8 rational components for 23 channels, and then the RFE method was applied to reduce the features, and these features were applied to LR, RF, and linear SVM.

Unlike existing approaches that often rely on black-box models or generic feature sets, this proposed work introduces a novel SHAP-based framework that emphasizes both patient-specific and patient-non-specific feature selection. The integration of explainability, optimization, and robust validation makes it not only more transparent but also more adaptable for clinical application, addressing a critical need for reliable and interpretable seizure detection solutions.

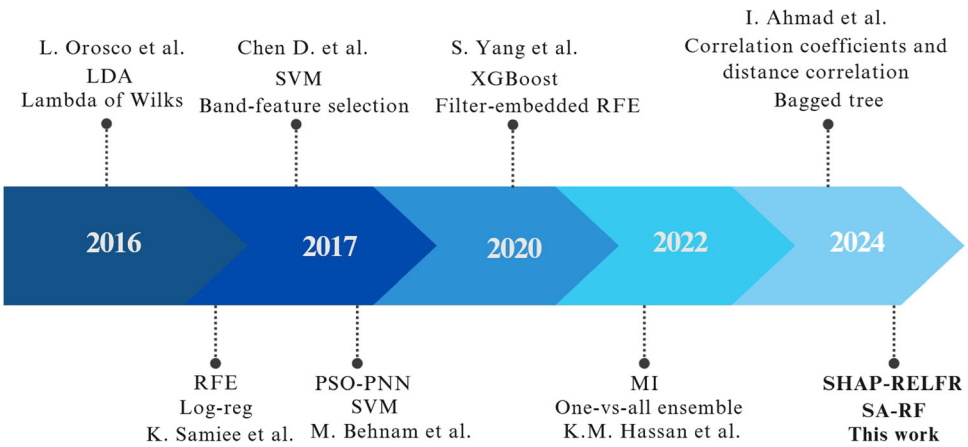

Fig. 1 Existing works on feature selection using CHB-MIT dataset

Materials and methods

This section encapsulates the tools and processes employed in the proposed seizure detection framework.

Proposed approach

Epileptic seizures are known to exhibit highly chaotic patterns that include complex spike-wave patterns (Sanei and Chambers 2013) and high voltage spikes (Sundaram et al. 1999). Considering this fact, this proposed novel framework, as depicted in Fig. 2, attempts to classify the multichannel EEG signal into seizure and non-seizure segments. The processing steps involved in this proposed work are explained in the following subsection. The experimentation is carried out on the CHB-MIT and Seina multichannel EEG datasets, as described in the next subsection.

EEG dataset

This proposed work has utilized two datasets, CHB-MIT and Seina, to evaluate the effectiveness of the proposed approach.

CHB-MIT dataset

The CHB-MIT scalp multichannel EEG dataset (Shoeb et al. 2004; Shoeb and Guttag 2010; Shoeb 2009) used in this work contains recordings of 24 pediatric patients with ages ranging from 1.5 to 22 years. Table 1 shows the detailed information about the patients included in the dataset.

This database was generated and donated to Physionet by Children's Hospital Boston (CHB) and Massachusetts Institute of Technology (MIT). This dataset is accessible online at physionet.org (Goldberger et al. 2000; PhysioNet 2010). The scalp EEG recordings from pediatric individuals were captured using a sampling frequency of 256 Hz with a 16-bit resolution. The international 10–20 EEG electrode placement system was used to record the EEG signals.

Seina dataset

This dataset comprises EEG recordings of epileptic patients, collected at the Unit of Neurology and Neurophysiology, University of Siena. This dataset is accessible

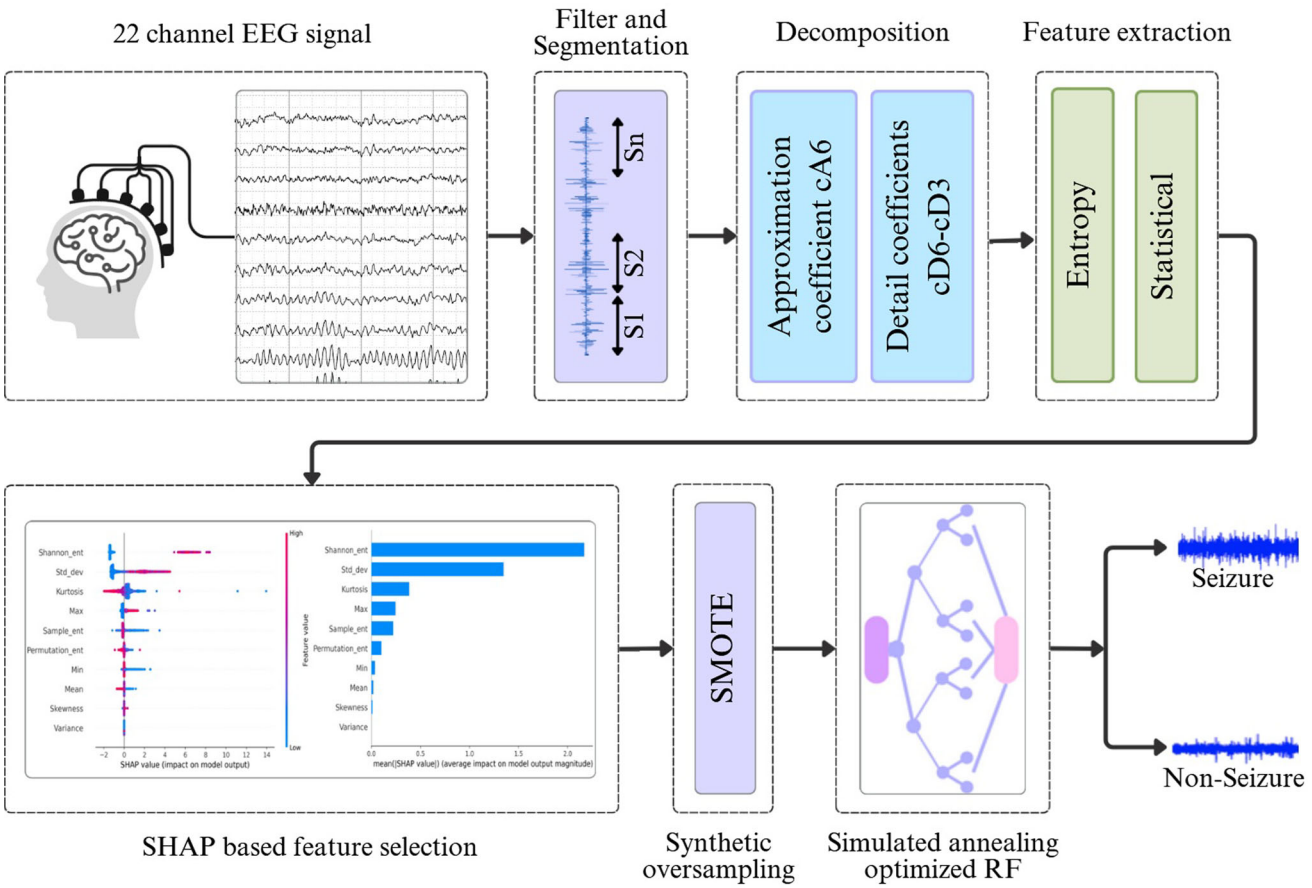

Fig. 2 The block diagram of the proposed framework for seizure detection demonstrating pre-processing, signal decomposition, feature extraction, feature selection, synthetic oversampling, and classification

Table 1 CHB-MIT scalp EEG dataset used in this proposed work

PID	Gender/age (years)	Number of seizures	Seizure duration (seconds)
Patient 1	F/11	7	442
Patient 2	M/11	3	172
Patient 3	F/14	7	402
Patient 4	M/22	4	378
Patient 5	F/7	5	558
Patient 6	F/1.5	10	153
Patient 7	F/14.5	3	325
Patient 8	M/3.5	5	787
Patient 9	F/10	4	276
Patient 10	M/3	7	447
Patient 11	F/12	3	806
Patient 12	F/2	40	1475
Patient 13	F/3	12	828
Patient 14	F/9	8	169
Patient 15	M/16	20	1992
Patient 16	F/7	10	69
Patient 17	F/12	3	293
Patient 18	F/18	6	317
Patient 19	F/19	3	236
Patient 20	F/6	8	294
Patient 21	F/13	4	199
Patient 22	F/9	3	204
Patient 23	F/6	7	424
Patient 24	–/–	16	511

online at physionet.org (PhysioNet 2020; Detti 2020; Detti et al. 2020). The participants include 9 males (ages 25–71) and 5 females (ages 20–58), monitored using Video-EEG with a 512 Hz sampling rate. EEG electrodes were placed following the international 10–20 system, and data acquisition was performed using EB Neuro and Natus Quantum LTM amplifiers with reusable silver/gold cup electrodes.

Data preparation

For the CHB-MIT time series dataset, the start time and end time of seizure events are provided in a separate text file. Throughout all experimentation 22 bipolar montage channels named as FP1-F7, F7-T7, T7-P7, P7-O1, FP1-F3, F3-C3, C3-P3, P3-O1, FP2-F4, F4-C4, C4-P4, P4-O2, FP2-F8, F8-T8, T8-P8, P8-O2, FZ-CZ, CZ-PZ, P7-T7, T7-FT9, FT9-FT10, FT10-T8 are utilized in this work. A total of 196 seizures are considered for experimentation purposes. The total duration of seizure considered is 3 h, 15 min, 57 s. The non-seizure samples of data are randomly selected from different files recorded at different times for a specific patient. This proposed work has considered every case as a patient.

In the Seina time series dataset, seizure event start and end times are recorded in a separate text file, formatted as hours, minutes, and seconds. The 28 EEG channels Fp1, F3, C3, P3, F7, T3, T5, Fc1, Fc5, Cp1, Cp5, F9, Fz, Cz, Pz, Fp2, F4, C4, P4, O2, F8, T4, T6, Fc2, Fc6, Cp2, Cp6, and F10 are used in this experimentation. Table 2 shows the details about the patients used in this proposed work. Seven patients from the Siena dataset are considered in this work. Patients PN00, PN06, PN09, PN10, PN12, PN13, and PN14 are designated as patient 1 to patient 7, respectively.

Filter and segmentation

The EEG signal from 22 channels of the CHB-MIT dataset and 28 channels of the Seina dataset is run through a 4th-order Butterworth low-pass filter with a cut-off frequency of 64 Hz. Further, it is applied to a notch filter having a cutoff frequency of 60 Hz for CHB-MIT and 50 Hz for the Seina dataset. These filters aid in mitigating the noise resulting from erroneous electrode placement, Sanei and Chambers (2021) skeletal muscle contractions, ocular blinks (Gotman and Gloor 1976), and interference from 60 Hz power lines (Rampil 1998; Sanei and Chambers 2013). In the passband, a Butterworth filter offers a maximum flat response. Following filtering, each EEG channel signal is divided into fixed-length segments with a duration of 4 s to make a signal statistically stationary (Sanei and Chambers 2021).

Decomposition using discrete wavelet transform (DWT)

The wavelet transform is a powerful tool for signal analysis that provides simultaneous localization in both time and frequency domains. Unlike the Fourier transform, which represents signals as infinite sine waves, the wavelet transform decomposes signals using small, finite-duration wavelets. This makes it particularly effective for analyzing non-stationary signals. DWT is a strong tool for signal decomposition analysis of non-stationary data (Rampil 1998), such as EEG (Strang and Nguyen 1996). A more thorough analysis of the signal's features is made possible by the DWT, which decomposes the signal into distinct components corresponding to particular frequency ranges. The DWT is a sampled version of the continuous wavelet transform (CWT), designed to analyze signals at multiple scales. The CWT for a signal $x(t)$ is defined as:

$$W(a,b) = \int_{-\infty}^{\infty} x(t) \frac{1}{\sqrt{a}} \psi\left(\frac{t-b}{a}\right) dt \quad (1)$$

where, $W(a, b)$ = wavelet coefficient at scale and translation, a = scaling parameter (controls frequency resolution),

Table 2 Seina scalp EEG dataset used in this proposed work

PID	Gender/age (years)	Number of seizures	Seizure duration (seconds)
Patient 1	M/55	5	325
Patient 2	M/36	5	282
Patient 3	F/27	3	203
Patient 4	M/25	10	338
Patient 5	M/71	4	290
Patient 6	F/34	3	264
Patient 7	M/49	4	163

b = translation parameter (controls time localization), $\psi(t)$= mother wavelet function. For the DWT, the scaling and translation parameters are discretized as follows: $a = 2^j$, $b = k \cdot 2^j$ where, a = scale index (determines the frequency band), b = translation index (controls time shift). The approximation and detail coefficients are given as:

$$A_j[n] = \sum_k h[k-2n] \cdot x[k] \tag{2}$$

$$D_j[n] = \sum_k g[k-2n] \cdot x[k] \tag{3}$$

where, $A_j[n]$ = approximation coefficients at level j, $D_j[n]$= detail coefficients at level j, $h[k]$= low-pass filter coefficients, $g[k]$ = high-pass filter coefficients, and $x[k]$ =discrete-time signal.

This work has employed a 6-level DWT to further decompose the segmented signal into seven sub-bands to perform a multi-resolution analysis. The purpose of this decomposition is to capture both low and high frequency components of the signal across different time scales, which is particularly beneficial for analyzing non-stationary signals like EEG. The DWT is particularly suited for analyzing non-stationary biomedical signals like EEG, as it allows the extraction of both time and frequency information simultaneously. At each level of decomposition, the signal is split into approximation coefficients which represent the low-frequency, or coarse components and detail coefficients, which capture high-frequency, or fine details,. The Daubechies 4 (db4) wavelet is selected as the mother wavelet due to its smoothness, compact support, and good localization properties, making it well-suited for analyzing biomedical signals.

After decomposing the signal up to 6 levels, the coefficients Ca6, Cd6, Cd5, Cd4, Cd3, Cd2, and Cd1 are obtained. From these, the approximation coefficient Ca6 and detail coefficients Cd6, Cd5, Cd4, and Cd3 are retained for further feature extraction, while Cd1 and Cd2 are discarded. This selection effectively focuses the analysis on the low-frequency region below 64 Hz, which encompasses most of the clinically relevant EEG bands such as delta, theta, alpha, and beta that are typically associated with seizure patterns. These selected coefficients are derived from every segment of each EEG channel, forming the basis for extracting meaningful features used in the further steps of processing.

Feature extraction

Feature extraction is an essential stage in the analysis of EEG signals for seizure detection. The process involves obtaining meaningful attributes from the EEG signal (Gotman and Gloor 1976) that can help in distinguishing between seizure and non-seizure segments. The estimated wavelet coefficients Ca6, Cd6, Cd5, Cd4, and Cd3 together have formed a coefficient feature set for each segment. The feature vector contains seven statistical and three entropy-based features, forming a set of a total of ten features (Dokare and Gupta 2025). The measure of variability and dispersion of the wavelet coefficients can be understood using statistical features (Rampil 1998). The statistical features, like a minimum signal value, maximum signal value, mean, standard deviation, variance, skewness, and kurtosis of the coefficients, are determined. The complexity and irregularity of the signal are captured by entropy features. Hence, this proposed work has used entropy-based features like sample entropy (Richman and Moorman 2000), permutation entropy (Bandt and Pompe 2002), and Shannon entropy (Acharya et al. 2018) of the wavelet coefficients along with statistical features. Combining two sets of features provides a richer and more detailed characterization of EEG signals, which aids in the identification of seizure patterns. These features are defined as follows:

$$Minimum = min\{x_1, x_2, \ldots, x_n\} \tag{4}$$

$$Maximum = max\{x_1, x_2, \ldots, x_n\} \tag{5}$$

$$Mean = \bar{x} = \frac{1}{n}\sum_{i=1}^{n} x_i \tag{6}$$

$$Variance = \frac{\sum (x_i - \bar{x})^2}{n} \tag{7}$$

$$Standard\ deviation = \sqrt{\frac{\sum (x_i - \bar{x})^2}{n}} \tag{8}$$

$$Skewness = g_1 = \frac{m_3}{m_2^{\frac{3}{2}}} \tag{9}$$

where $m_3 = \frac{1}{n}\sum_{i=1}^{n}((x_i - \bar{x})^3)$ and $m_2 = \frac{1}{n}\sum_{i=1}^{n}((x_i - \bar{x})^2)$

$$Kurtosis = \frac{1}{n}\frac{\sum_{i=1}^{n}(x_i - \bar{x})^4}{S^4} \tag{10}$$

Consider a time-series data set of length $N = \{x_1, x_2, x_3, \ldots, x_N\}$, a template vector of length m, such that $X_m(i) = \{x_i, x_{i+1}, x_{i+2}, \ldots, x_{i+m-1}\}$ and the distance function $d[X_m(i), X_j](i \neq j)$ is to be the Chebyshev distance, then

$$Sample\ entropy = E_s = -\ln\frac{a}{b} \tag{11}$$

a and b are number of template vector pairs having $d[X_{m+1}(i), X_{m+1}(j)] < r$ and $d[X_m(i), X_m(j)] < r$ respectively. Where N is the number of data points, m is an embedding dimension, and r is the tolerance. For a time series data, let p be a probability distribution associated with it, where π_i are the frequencies associated with i possible permutation patterns and D is the embedding dimension, therefore $i = 1, 2, \ldots, D!$.

$$Permutation\ entropy = E_p = -\sum_{i=1}^{D!}\Pi_i \log_2 \Pi_i \tag{12}$$

$$Shannon\ entropy = E_{sh}(X) = -\sum_{i=1}^{N} p(x_i)\log_2 p(x_i) \tag{13}$$

where $p(x_i)$ is the probability occurrence of feature values from x_1 to x_N.

SHAP values for feature selection

The dimensionality of the feature space rises with the number of features included, making it more challenging for machine learning models to prevent overfitting and achieve good generalization. By choosing a subset of the most useful features (Cunningham 2008), feature selection helps to overcome this problem (Kondo et al. 2019). Ten features per channel indicate diverse features extracted from the EEG signal. Due to the variability in seizure patterns among patients, not all ten features may effectively distinguish between seizure and non-seizure segments. The diversity in features helps capture different aspects of neural activity related to seizures. While rich feature spaces add complexity to the model, they may include redundant or non-informative features for seizure detection. Intense computing demands might arise when training machine learning models on a high-dimensional feature space (Cunningham 2008). SHAP is a powerful tool in the field of Explainable AI (XAI) (Frasca et al. 2024), offering valuable insights into how models make their predictions and serving as a viable option for feature selection by attributing contributions of each feature to the model's output in a transparent and interpretable manner.

SHAP (SHapley Additive exPlanations) (Shapley 1953) is an advanced interpretability method that explains how individual input features contribute to a machine learning model's prediction (Ahmad et al. 2024; Lundberg and Lee 2017; Tallón-Ballesteros and Chen 2020). It is based on the concept of Shapley values from cooperative game theory, originally designed to fairly distribute payouts among players depending on their contributions to a collective result.

In the context of machine learning, SHAP treats each feature as a player in a game where the goal is to predict an outcome. For any given input instance, SHAP computes how much each feature has contributed to pushing the model's output away from the average prediction (called the expected value) of the model. To calculate a SHAP value for a feature, the method considers all possible combinations (subsets) of the other features and evaluates the model's output with and without the presence of the target feature. The average of all these marginal contributions, weighted by the size of the subset, gives the SHAP value (Lundberg and Lee 2017). This ensures a fair and mathematically consistent way of attributing importance.

SHAP values uphold several important theoretical properties that make them a reliable and consistent tool for model interpretability. One such property is local accuracy, which ensures that the sum of all SHAP values for a particular instance equals the model's actual prediction for that instance. This guarantees that the explanation fully accounts for the output. Another key property is missingness, meaning that if a feature is not present in the model or not used in a particular prediction, it is assigned a SHAP value of zero, indicating no contribution. Lastly, consistency ensures that if a model changes in such a way that a feature contributes more to the prediction, the SHAP value for that feature does not decrease. Together, these properties provide a solid mathematical foundation for SHAP's fairness, reliability, and interpretability in explaining complex model behavior.

The SHAP package of Python is used to estimate the SHAP values and rank the features based on their importance. This proposed work has employed a TreeExplainer, a tree-based model, and a probability-based link function. Features that have greater absolute SHAP values are considered to have a greater impact on model predictions. For each feature in the feature set, the mean absolute SHAP values for all samples are calculated. These SHAP values indicate the relative contribution of each feature to the model predictions. Based on the mean absolute SHAP values, the top features are chosen that had the biggest

impact on the model predictions. The number of features that were chosen had been determined empirically to reduce dimensionality and maintain the most informative features. In the machine learning model f for seizure detection task with i features employed, and the value function $f_x(S)$ is typically the model's prediction when only features in subset S are used for instance x, the SHAP value ϕ_i (Tallón-Ballesteros and Chen 2020) is given as:

$$\phi_i = \sum_{S \subseteq F \setminus \{i\}} \frac{|S|!.(|F|) - (|S|-1)!}{|F|!} [f_x \cup \{i\} - f_x(S)] \quad (14)$$

where

- F is the set of all features.
- S is a subset of features without i.
- $f_x(S)$ is model output with subset S.
- $f_x \cup \{i\}$ is model output with subset S plus feature i.

In this proposed work, SHAP is used not just to interpret model outputs, but also for feature selection by identifying and ranking features that contribute the most to seizure detection in EEG data. This use of SHAP ensures that selected features are not only statistically significant but also clinically interpretable, offering transparency in a typically black-box system. This makes SHAP particularly valuable in critical applications like healthcare, where understanding model decisions is as important as their accuracy.

This proposed work has carried out two experiments for feature selection. The first one involves selecting patient-specific features using the SHAP value, and the second is a novel proposed SHAP-RELFR method that determines a common set of features from the patient-specific feature ranking and its relative frequency.

SHAP-based patient-specific feature selection

In the case of patient-specific feature selection, the feature ranking is determined for each patient independently, and the model of that patient will use those features for classification. For calculating the SHAP value of each feature, RF classification model is trained using a dataset containing 10 features extracted from 22 EEG channels of CHB-MIT and 28 channels of Seina dataset. This trained RF model is used to calculate SHAP values, which measure the contribution of each feature to the model's predictions. The global importance of each feature is calculated by averaging the SHAP values across every instance used for training.

$$SHAP\ importance(i) = \frac{1}{M} \sum_{j=1}^{M} |\phi_{i,j}| \quad (15)$$

where M is the number of samples, and $\phi_{i,j}$ is the SHAP value for feature i in sample j.

Following that, the features are ranked according to their mean absolute SHAP values for each patient. All ten features are ranked according to their feature importance from rank R1 to R10. The top 5 and top 3 features are selected for further analysis.

Patient-non-specific feature selection using SHAP-RELFR method

This work has proposed a novel method, SHAP-RELFRF to determine common features that are employed to train a model for all patients. Once the patient-specific feature ranking is obtained using SHAP values, the features common to all patients are estimated using a relative frequency (RELFR) of features ranked. Figure 3 presents the flow chart of the proposed SHAP-REFLR method. The feature importance for each patient is estimated using the SHAP value before the application of this algorithm and ranked from 1 to 10. The features are numbered as 0: Min, 1: Max, 2: Mean, 3: Variance, 4: Std_dev, 5: Kurtosis, 6: Skewness, 7: Sample_ent, 8: Permutation_ent, 9: Shannon_ent. The algorithm starts by initializing feature F as 0 and ranking R as 1. In this implementation, rank 5 and a total of 10 features are taken into account. The frequency of occurrence of every feature under each rank across all patients is estimated. Further, the percentage of occurrence of every feature under each rank across all patients is determined. This percentage of occurrence provides the feature importance irrespective of the patient.

The features with a non-zero value of percentage of feature importance can be selected under rank 1 since the features under the rank 1 category are fewer in number and contribute more to seizure detection.

Synthetic minority oversampling technique (SMOTE)

In many real-world classification problems, especially in medical and biomedical domains like seizure detection, datasets often suffer from class imbalance. This means that one class (typically the normal or non-seizure class) contains significantly more samples than the other class (e.g., seizure events). When a classifier is trained on such data, it tends to favor the majority class, leading to poor detection performance for the minority class, which is often the clinically important one.

To address this issue, the Synthetic Minority Oversampling Technique (SMOTE) (Chawla et al. 2002) is employed as a data-driven approach for class balancing (Fernández et al. 2018). SMOTE is an oversampling technique that creates new synthetic samples for the minority class rather than merely duplicating existing ones. The key idea is to expand the feature space of the minority

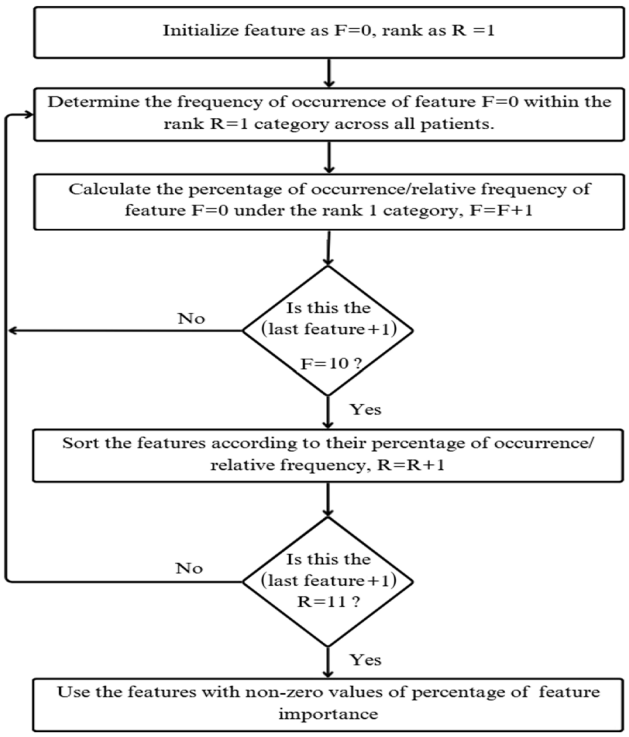

Fig. 3 Flow chart of SHAP-RELFR method for patient-non-specific feature selection

class in a more meaningful and generalized way, helping the classifier to better learn its characteristics. It generates new samples by interpolating between existing samples of the minority class. For each minority class instance, SMOTE identifies its k nearest neighbors within the same class. It then randomly selects one of these neighbors and creates a new synthetic data point along the line segment that connects the original sample and the selected neighbor. This process introduces new and realistic samples that lie within the feature space of the minority class, thereby helping to balance the dataset and improve model performance, particularly in cases of class imbalance. This results in a more generalized decision boundary and helps prevent overfitting that often arises from mere replication.

When addressing class imbalance using SMOTE, it is critical to apply the method correctly within the model evaluation pipeline, particularly during cross-validation, to avoid data leakage. Data leakage occurs when information from outside the training data influences the model during evaluation, leading to artificially inflated performance metrics and unreliable results. We have employed SMOTE exclusively on the training data within each 5 cross-validation folds to address class imbalance without introducing data leakage. This is implemented by integrating SMOTE into a machine learning pipeline along with the classifier. The pipeline ensures that, for every fold during cross-validation, SMOTE is applied only to the training subset, and the model is evaluated on the test subset.

This approach preserves the independence of the test data, avoids contamination from synthetic samples, and provides performance metrics that accurately reflect the model's ability to generalize to unseen data.

Classification

An overall feature vector is formed by concatenating the data of selected features from 22 channels or 28 channels. The seizure segment is labeled as '1' and the non-seizure segment as '0'. The final feature set is shuffled and divided into 70%-30% as the training–testing set.

Simulated annealing (SA) optimized RF

After data splitting, the RF classifier is trained using the training data. The selection of hyperparameters significantly impacts how well RF classifiers function. Conventional techniques, such as grid search, may not necessarily produce the best results and can be computationally expensive. A more effective method is provided by simulated annealing (SA), which explores the hyperparameter space adaptively (Gandomi et al. 2013). In this work, we propose the SA method to optimize the hyperparameters of RF classifiers. SA is a powerful metaheuristic optimization method created based on the actual metallurgical process of annealing (Gandomi et al. 2013; Van Laarhoven 1987). This probabilistic optimization approach involves heating and then progressively cooling a material to remove defects and enhance its crystalline structure (Suman and Kumar 2006). To solve combinatorial optimization issues, Kirkpatrick (1983) initially presented this approach in 1983. By concentrating on promising areas of the hyperparameter space, SA can decrease the number of evaluations needed and raise the possibility of locating optimal or nearly optimal solutions. This is made possible by the probabilistic acceptance criterion. The main aim of SA is to minimize (or maximize) an objective function $f(x)$ where x represents a set of variables or hyperparameters. The steps in the simulated annealing algorithm are as follows:

1. Set the initial hyperparameters as x_0 and compute the objective function value $f(x_0)$.
2. Set an initial temperature as T_0 that controls the probability of accepting worse solutions.
3. Define a cooling rate α. Update the temperature T_k for every k iteration such that $T_{k+1} = \alpha T_k$.
4. Generate a neighboring solution x' by slightly modifying the current solution x.

5. Determine the change in the objective function value $\Delta E = f(x') - f(x)$. If $\Delta E < 0$, then accept x'; otherwise, accept x' with probability P.
6. Update the current solution x to the new solution x' if accepted. Repeat the process, reducing the temperature according to the cooling schedule, until a stopping criterion is met.

The value of hyperparameters n_estimators, max_depth, initial_temperature, cooling_rate, and max_iterations are considered as 50, 5, 100, 0.95, and 100, respectively.

Performance metrics

The effectiveness of classifiers in discriminating between seizure and non-seizure segments is evaluated by estimating metrics such as accuracy, precision, specificity, sensitivity, F1-score, and AUC score. These metrics are defined based on the confusion matrix values as true positive (TP), true negative (TN), false positive (FP), and false negative (FN). The performance metrics used are defined as follows:

Accuracy: This measure summarises the model's performance across two classes. It is a ratio of the number of correctly classified labels to the total number of labels.

$$Accuracy = \frac{TP + TN}{TP + TN + FP + FN} \tag{16}$$

Precision/PPV: This metric gauges how well the model classifies a label as positive. It is a ratio of correctly classified seizure segments to the total number of segments classified as seizure (correctly or incorrectly). High precision means fewer false positives.

$$Precision/PPV = \frac{TP}{TP + FP} \tag{17}$$

where PPV is the positive predictive value.

Sensitivity/Recall/TPR: It refers to how many of the actual seizure segments can be predicted correctly by the model. The ratio of correctly predicted seizure segments to all actual seizure segments.

$$Sensitivity/Recall/TPR = \frac{TP}{TP + FN} \tag{18}$$

where TPR is the true positive rate.

Specificity/Selectivity/TNR: It is a ratio of the number of correctly detected non-seizure segments to the total number of actual non-seizure segments.

$$Specificity/selectivity/TNR = \frac{TN}{TN + FP} \tag{19}$$

where TNR is the true negative rate.

F1-score: It is a harmonic mean of recall and precision. It balances both metrics, especially when the dataset is imbalanced.

$$F1 - score = 2\frac{precision * recall}{precision + recall} = \frac{TP}{TP + \frac{1}{2}(FP + FN)} \tag{20}$$

Area Under the Receiver Operating Characteristic Curve (AUC-ROC): It is one of the most widely used metrics in medical diagnosis. It assesses a classifier's ability to distinguish between two classes.

Experimental results and analysis

All experiments are carried out using the CHB-MIT and Seina datasets on an 11th-generation i5 processor with 16 GB of RAM. For every patient in the dataset, an independent experiment is conducted.

Results of feature selection

After obtaining the statistical and entropy-based features, an individual model is trained for each patient, and the feature ranking is obtained in each case. This section covers the results obtained from patient-specific and patient-non-specific feature selection approaches.

Results of SHAP-based patient-specific feature selection

The results of feature selection for each patient are described in this section. The SHAP values obtained for features Min, Max, Mean, Variance, Std_dev, Kurtosis, Skewness, Sample_ent, Permutation_ent, and Shannon_ent for both datasets are shown in Fig. 4. The summary plots in Fig. 4(a) and Fig. 4(b) show the features ranked for patient 1 as per the importance score estimated using the SHAP values using CHB-MIT and Seina datasets, respectively. A wider spread of dots for feature Shannon_ent indicates that it has a greater influence on the model's predictions for patient 1 across both datasets. Feature Shannon_ent exhibits the highest SHAP value, whereas feature Variance shows the lowest across both datasets, as depicted in Fig. 4. For model interpretation and feature selection, the SHAP summary bar graph is an effective way to visualize feature importance, as shown in Fig. 5. This SHAP summary bar graph illustrates the average absolute impact of each feature on the model's output. Shannon_ent, represented by the first bar, exhibits the highest mean SHAP value, indicating that it is the most influential feature in the model's prediction process for both datasets. In contrast, Variance, positioned last, has zero SHAP value, suggesting minimal contribution to the model's output. This ranking reflects the relative importance of features, where higher bars signify stronger influence, aiding in interpretability in feature selection decisions.

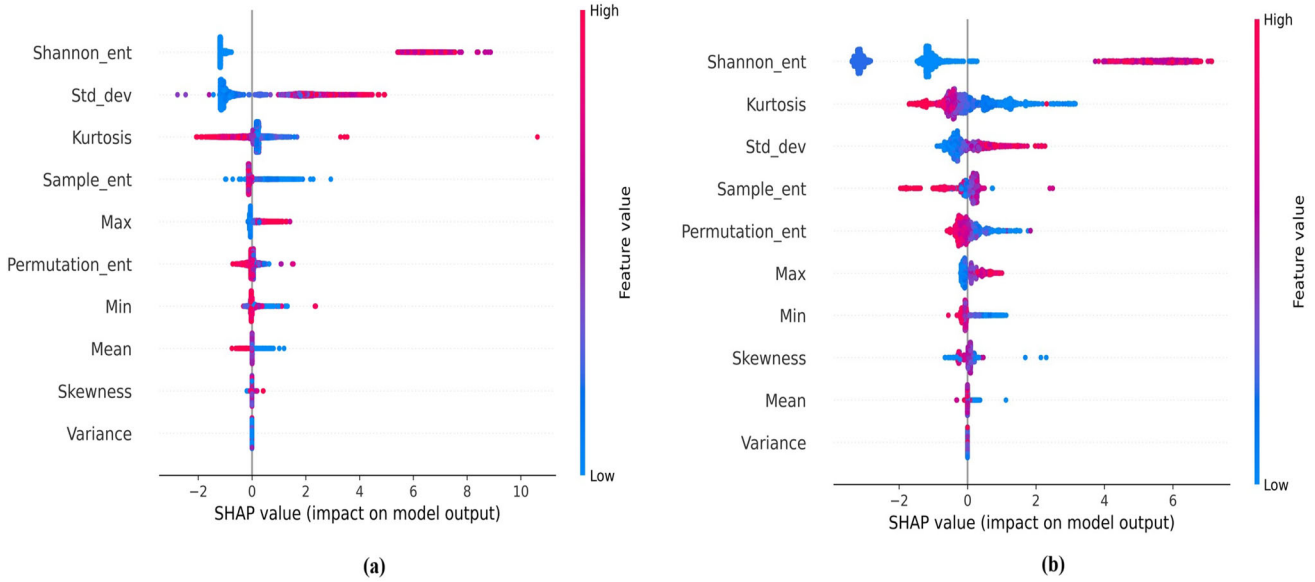

Fig. 4 SHAP summary plots illustrating the contribution of features towards seizure classification for patient 1 using **a** the CHB-MIT dataset and **b** the Siena dataset. The color gradient represents the feature value (low to high), while the horizontal axis indicates the SHAP value, reflecting the impact of each feature

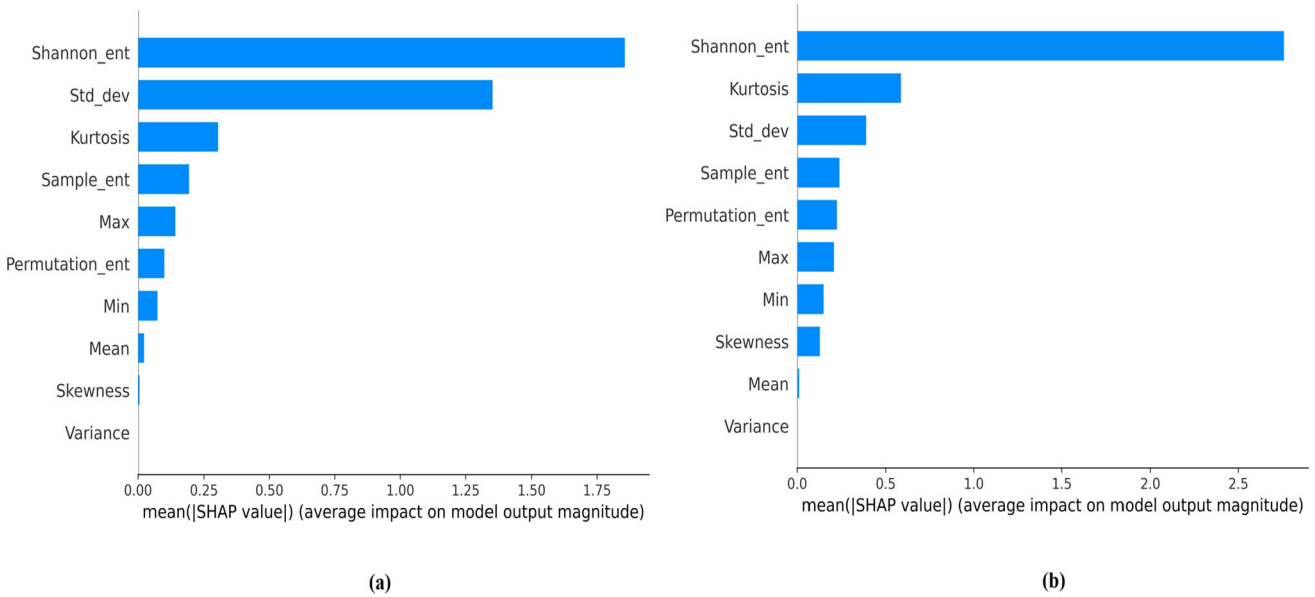

Fig. 5 SHAP summary bar graphs showing the average feature importance for seizure classification in patient 1 using **a** the CHB-MIT dataset and **b** the Siena dataset. The bars represent the mean absolute SHAP values, indicating the overall contribution of each feature to the model's predictions

This kind of graph highlights the features that most influence the model's predictions by ranking them according to their mean absolute SHAP values. The feature ranking obtained for patients of the CHB-MIT and Seina datasets is presented in Tables 3 and 4, respectively. Feature Min is represented by the number 0 and feature Shannon_ent by the number 9. Tables 3 and 4 show that the feature importance rankings obtained through SHAP value analysis demonstrate a notable level of consistency across both the CHB-MIT and Siena datasets. This observation indicates that the model identifies and leverages similar underlying patterns and discriminative features in both datasets, regardless of potential variations in patient profiles or recording conditions. Such consistency reinforces the robustness and generalizability of the selected features, highlighting their relevance in accurately

Table 3 Feature ranking obtained using the SHAP value for each patient in the CHB-MIT dataset

PID	Feature rank									
	Top 5									
	Top 3									
	R1	R2	R3	R4	R5	R6	R7	R8	R9	R10
Patient 1	9	4	5	1	7	8	0	2	6	3
Patient 2	9	4	0	1	5	7	2	6	8	3
Patient 3	4	9	0	1	7	5	8	2	6	3
Patient 4	4	9	1	5	8	7	0	6	2	3
Patient 5	7	9	4	5	8	0	6	1	2	3
Patient 6	7	9	4	5	6	8	1	0	4	3
Patient 7	9	7	8	4	1	5	0	2	6	3
Patient 8	9	4	0	7	1	6	5	8	4	3
Patient 9	4	0	8	1	2	9	7	5	6	3
Patient 10	9	4	7	5	8	0	1	6	2	3
Patient 11	4	0	1	7	5	8	6	9	2	3
Patient 12	9	5	7	8	4	0	1	6	2	3
Patient 13	9	7	8	5	4	1	6	0	2	3
Patient 14	9	7	5	8	4	1	0	6	2	3
Patient 15	9	4	1	5	0	7	8	6	2	3
Patient 16	9	7	4	8	1	0	5	2	6	3
Patient 17	9	4	7	5	8	1	0	2	6	3
Patient 18	4	9	1	0	6	5	8	7	2	3
Patient 19	9	7	5	6	8	0	1	4	3	2
Patient 20	9	8	7	6	5	0	1	4	2	3
Patient 21	9	4	7	0	6	8	5	1	2	3
Patient 22	4	7	9	0	2	1	8	6	5	3
Patient 23	9	7	4	5	0	1	8	6	2	3
Patient 24	9	4	7	5	1	0	8	2	6	3

PID: Patient ID, **R1 to R10**: Rank 1 to rank 10, Numbers 0 to 10 indicates feature numbers, 0: Min, 1: Max, 2: Mean, 3: Variance, 4: Std_dev, 5: Kurtosis, 6: Skewness, 7: Sample_ent, 8: Permutation_ent, 9: Shannon_ent

Table 4 Feature ranking obtained using the SHAP value of patients in the Seina dataset

PID	Feature rank									
	Top 5									
	Top 3									
	R1	R2	R3	R4	R5	R6	R7	R8	R9	R10
Patient 1	9	5	4	7	8	1	0	6	2	3
Patient 2	9	4	7	1	5	8	0	6	2	3
Patient 3	9	4	0	8	1	5	7	6	2	3
Patient 4	9	7	4	5	0	1	6	8	2	3
Patient 5	9	7	6	0	1	4	8	5	2	3
Patient 6	9	7	5	8	6	0	4	1	2	3
Patient 7	9	4	0	5	6	1	2	8	7	3

Table 5 Patient-non-specific feature estimation: feature importance obtained in percentage under the category rank 1 to rank 5 across all 24 patients from the CHB-MIT dataset

Features	Feature importance in percentage				
	Rank 1	Rank 2	Rank 3	Rank 4	Rank 5
Shannon_ent	66.7	20.8	4.17	0	0
Std_dev	25	33.3	16.7	4.2	12.5
Sample_ent	8.33	29.2	25	8.3	8.3
Kurtosis	0	4.17	12.5	37.5	12.5
Max	0	0	16.7	16.7	16.7
Min	0	8.3	12.5	12.5	8.3
Permutation_ent	0	0	12.5	12.5	20.8
Skewness	0	0	0	8.3	12.5
Mean	0	0	0	0	8.3
Variance	0	0	0	0	0

distinguishing between seizure and non-seizure activities across different datasets. The top 5 and the top 3 features are selected based on their ranking. Three feature sets are formed for every patient for further analysis are F10, F5, and F3. Feature set F10 contains 10 original features, F5 contains the top 5 selected features, and F3 contains the top 3 features.

As shown in Table 3, when feature Shannon_ent is considered, it is observed to occur 16 times out of 24 cases of the CHB-MIT under the rank 1 (R1) category, yielding an occurrence of 66.7%. Similarly, Std_dev and Sample_ent have obtained occurrences of 25% and 8.33%, respectively under the category rank 1. Considering all 24 cases, Shannon_ent has attained maximum feature importance in percentage under category rank 1, indicating this single feature effectively contributes to seizure detection for all patients. To apply a final feature set to the classifier for all patients, features with non-zero values under the category rank 1 are considered. Hence, Shannon_ent, Std_dev, and Sample_ent are three features selected as common features for all patients.

In the case of the Seina dataset, as shown in Table 4, Shannon_ent has ranked 1 across all patients, and Variance has ranked last. As shown in Tables 3 and 4, although the ranking of a few individual features differs slightly between the CHB-MIT and Seina datasets, the overall trend in feature importance remains largely consistent. As illustrated in Table 4, Shannon_ent has ranked 1 across all patients, yielding an occurrence of 100% under the

Table 6 Patient-non-specific feature estimation: feature importance obtained in percentage under the category rank 1 to rank 5 for 7 patients from the Seina dataset

Features	Feature importance in percentage				
	Rank 1	Rank 2	Rank 3	Rank 4	Rank 5
Shannon_ent	100	0	0	0	0
Std_dev	0	42.86	28.56	0	0
Sample_ent	0	42.86	14.29	14.29	0
Kurtosis	0	14.29	14.29	28.56	14.29
Max	0	0	0	14.29	28.56
Min	0	0	28.56	14.29	14.29
Permutation_ent	0	0	0	28.56	14.29
Skewness	0	0	14.29	0	28.56
Mean	0	0	0	0	0
Variance	0	0	0	0	0

category rank 1. Whereas, Sample_ent, Std_dev and Kurtosis have obtained occurrences of 42.86%, 42.86% and 14.29% respectively under the category rank 2.

The patient-specific features obtained are further utilized to derive patient-non-specific features through the proposed novel SHAP-RELFR methodology.

Results of SHAP-RELFR patient-non-specific feature selection

The patient-non-specific features selected for the CHB-MIT dataset and the Seina dataset using our proposed SHAP-RELFR method are depicted in Tables 5 and 6, respectively. This has determined the overall ranking of each feature across all patients using the findings reported in Tables 3 and 4. As reported in Tables 3 and 4, the ranking of each feature for each patient indicates the importance of that feature in the seizure discrimination task. For instance, feature 9 (Shannon entropy), which is ranked under Rank 1 (R1), is the most important for most of the patients of the CHB-MIT dataset and all patients of the Seina dataset.

To obtain the patient independent ranking of the feature, the occurrence of each feature under each rank (R1 to R10) is determined. For the CHB-MIT dataset, feature 9 has occurred 16 times out of a total of 24 cases. A similar process is followed for other features by referring the Table 3. Since the main objective is to reduce the feature dimension, the top 5 ranking values are considered for the estimation of the patient independent features. After determining the occurrence of a feature within a certain category (rank 1 to rank 5), the percentage of occurrence/relative frequency of each feature is estimated from a total of 24 patients of the CHB-MIT dataset. Hence, the feature importance of feature 9 (Shannon_ent) in percentage is estimated as 66.7, while for feature 4 (Std_dev) and feature 7 (Sample_ent), the feature importance in percentage is 25 and 8.33, respectively. And, the other features have an importance score of zero under the Rank 1 category. A similar procedure is followed to obtain the feature importance of each feature under other categories. The final selected features for patient-non-specific approach using our proposed novel approach are Shannon_ent, Std_dev, and Sample_ent. We have considered features obtained under the Rank 1 category, since the number of features under this category will be the least in number.

For the Seina dataset, as illustrated in Table 6, feature 9 (Shannon_ent) consistently ranked 1 across all 7 patients, achieving a feature importance score of 100%. Similarly, feature 7 (Sample_ent), feature 4 (Std_dev), and feature 5 (Kurtosis) are identified under the rank 2 category, with each obtaining a feature importance score of 42.86%, 42.86%, and 14.29%, respectively. In the patient-non-specific approach, we selected features from both rank 1 and rank 2 categories. As a result, the final set of common features applied across all 7 patients includes: Shannon_ent, Sample_ent, Std_dev, and Kurtosis.

The effectiveness of the selected features is validated by evaluating their performance using a Simulated Annealing-optimized Random Forest (SA-RF) classifier.

Results of classification

The results obtained using this proposed approach for both patient-specific and patient-non-specific feature selection are evaluated by applying the selected features to a SA-RF classifier. This section presents a comparative analysis of the results obtained with and without the application of SMOTE, aiming to evaluate its impact on model performance.

Classification results using patient-specific feature selection

Three experiments are conducted using three feature sets: F10, F5, and F3, applied individually to the SA-RF model for each patient in both datasets. The hyperparameters of the model are optimized using simulated annealing with 5-fold cross-validation. To ensure that the optimized hyperparameters are robust and do not overfit the training data, 5-fold cross-validation is used.

For the CHB-MIT dataset, the performance metrics obtained using feature sets F10, F5, and F3 with the application of SMOTE for each patient are illustrated in Fig. 6, Fig. 7, and Fig. 8. As shown in Fig. 6(a), the accuracy achieved with features F10 and F5 exceeds 93% for all patients, except for patient 15, where it is reduced by 5%.

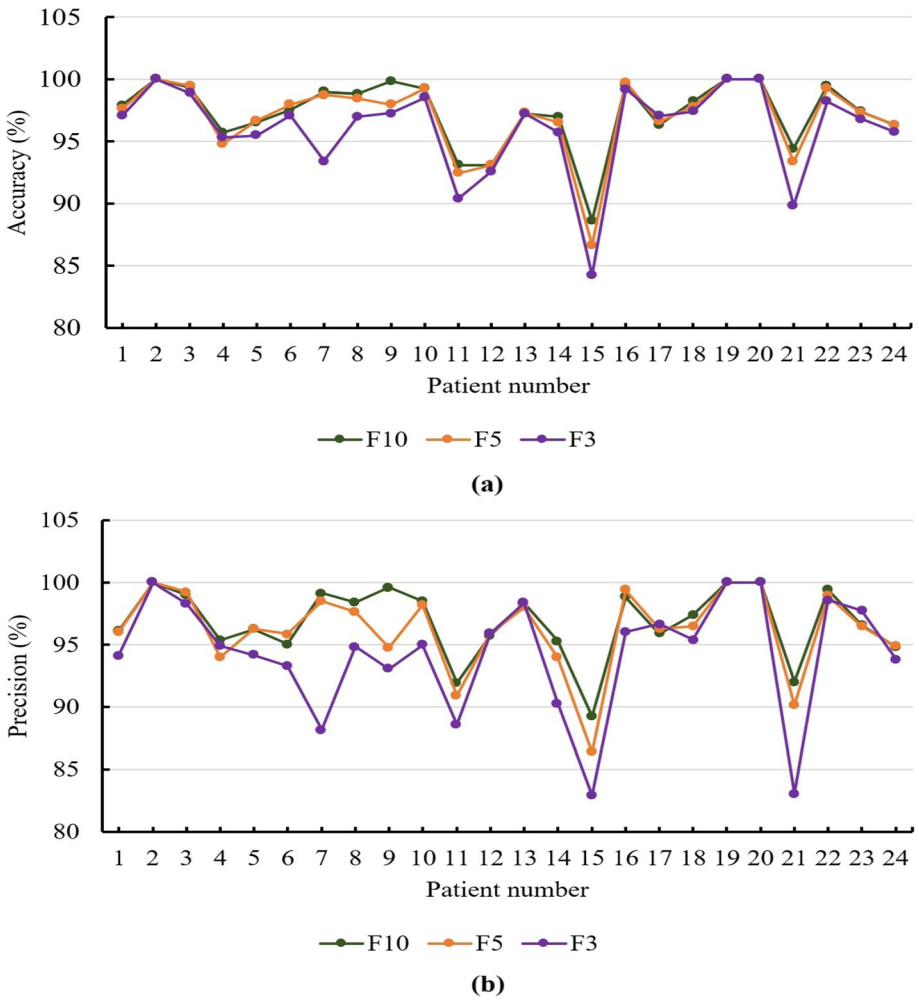

Fig. 6 Patient-specific feature selection with SMOTE applied to all patients from the CHB-MIT dataset using three feature sets: original 10 features (F10), top 5 features (F5), and top 3 features (F3). Results are presented for **a** Accuracy and **b** Precision

According to Fig. 6b, the precision achieved is greater than 90% for each patient when utilizing F10 and F5, except for 15. The sensitivity obtained is above 90% for all patients, except for patients 12, 15, and 21 when using F10, F5 and F3, as depicted in Fig. 7a. It is observed that all three feature sets show an almost similar trend across all patients.

However, as demonstrated in Fig. 7(b), the model's specificity remains exceptional across all cases, achieving a more than 96% for every patient except for patient 15 using F10 and F5. The F1-score obtained is greater than 90% using F10 and F5, except for patients 12 and 15, as illustrated in Fig. 8(a). Additionally, the AUC score exceeds 0.9 for all patients except for patients 12 and 15 when utilizing F10 and F5, as shown in Fig. 8(b).

Table 7 presents a detailed comparison of average performance metrics for seizure detection using three feature sets, original 10 features (F10), top 5 features (F5), and top 3 features (F3), which are evaluated with and without the application of SMOTE. This analysis highlights the impact of feature reduction and oversampling on classification performance. Notably, even with reduced feature sets (F5 and F3), the model maintains comparable accuracy, precision, and AUC to the original F10, indicating that feature reduction does not significantly compromise performance. The application of SMOTE further enhances the results, particularly in terms of sensitivity and F1-score, which are crucial for reliable seizure detection.

For instance, the sensitivity improves from 85.26 to 94.03% for F3 and from 87.90 to 95.08% for F10 when SMOTE is applied. Although a slight decrease in specificity is observed with SMOTE, the overall classification ability remains strong. These findings suggest that effective feature selection, combined with SMOTE, can lead to efficient and accurate seizure detection using fewer features, supporting the goal of computational efficiency without sacrificing diagnostic performance.

In the case of the Seina dataset, the performance metrics obtained using the original 10 features (F10), the top 5 selected features (F5), and the top 3 selected features (F3) by the application of SMOTE are illustrated in Fig. 9. The accuracy for patients 1, 4, 6, and 7 exceeds 95%, while for patients 2, 3, and 5 it remains above 91%, as depicted in

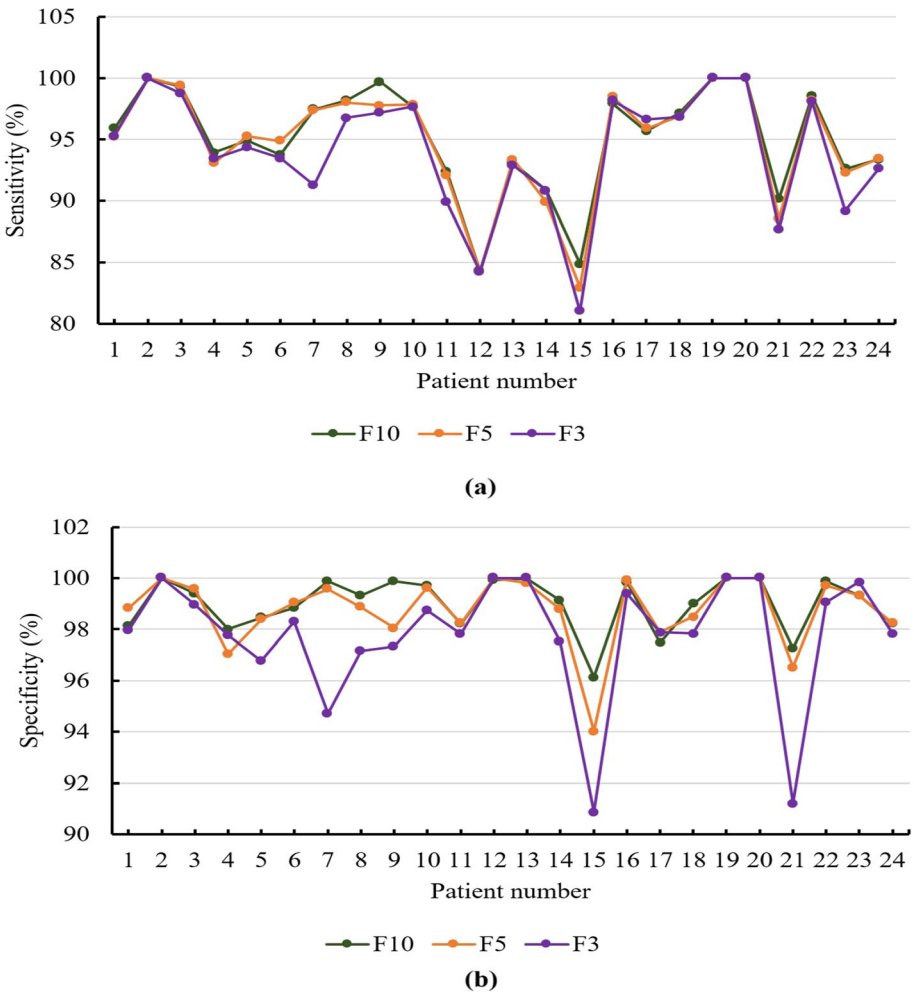

Fig. 7 Patient-specific feature selection with SMOTE applied to all patients from the CHB-MIT dataset using three feature sets: original 10 features (F10), top 5 features (F5), and top 3 features (F3). Results are presented for **a** Sensitivity and **b** Specificity

Fig. 9(a). Precision results, shown in Fig. 9b, indicate that patients 1, 4, 6, and 7 maintain values above 95%, whereas patients 2 and 3 achieve over 91%. The sensitivity values, presented in Fig. 9c, reveal a maximum of 98% and a minimum of 89% for patients 2 and 3. As demonstrated in Fig. 9d, the specificity ranges from 92 to 100%. Figure 9e highlights F1-score values, which lie between 91% and 99%. Lastly, the AUC results span from 0.90 to 0.99, as illustrated in Fig. 9f.

Using the Seina dataset, Table 8 presents a comparative evaluation of classification performance with and without the application of SMOTE across three sets of features: the original 10 features (F10), the top 5 selected features (F5), and the top 3 selected features (F3). With SMOTE applied, the model shows slightly improved or consistent accuracy, precision, and sensitivity across all feature sets compared to the non-SMOTE scenario. For example, the average accuracy improved from 95.07% (F10 without SMOTE) to 95.27% (F10 with SMOTE), and the sensitivity increased from 93.53 to 94.46%. Similarly, the AUC values show a noticeable enhancement, reaching up to 0.9441 with SMOTE for F10, compared to 0.9372 without it. Importantly, even with reduced features (F5 and F3), the drop in performance metrics is minimal, indicating that the proposed feature reduction method retains significant discriminative power while reducing dimensionality. Overall, these results affirm that applying SMOTE enhances the robustness of the classifier, and reducing features does not significantly compromise the model's performance.

Classification results using patient-non-specific feature selection

As discussed in Section 4.1.2, the features Shannon_ent, Std_dev, and Sample_ent are selected under the rank 1 category for the patient-non-specific approach using the CHB-MIT dataset. These features, identified through our systematic and novel feature selection method, represent a common feature subset suitable for the seizure detection model across all patients in the CHB-MIT dataset. For the Seina dataset, the patient-non-specific feature set includes Shannon_ent, Std_dev, Sample_ent, and Kurtosis.

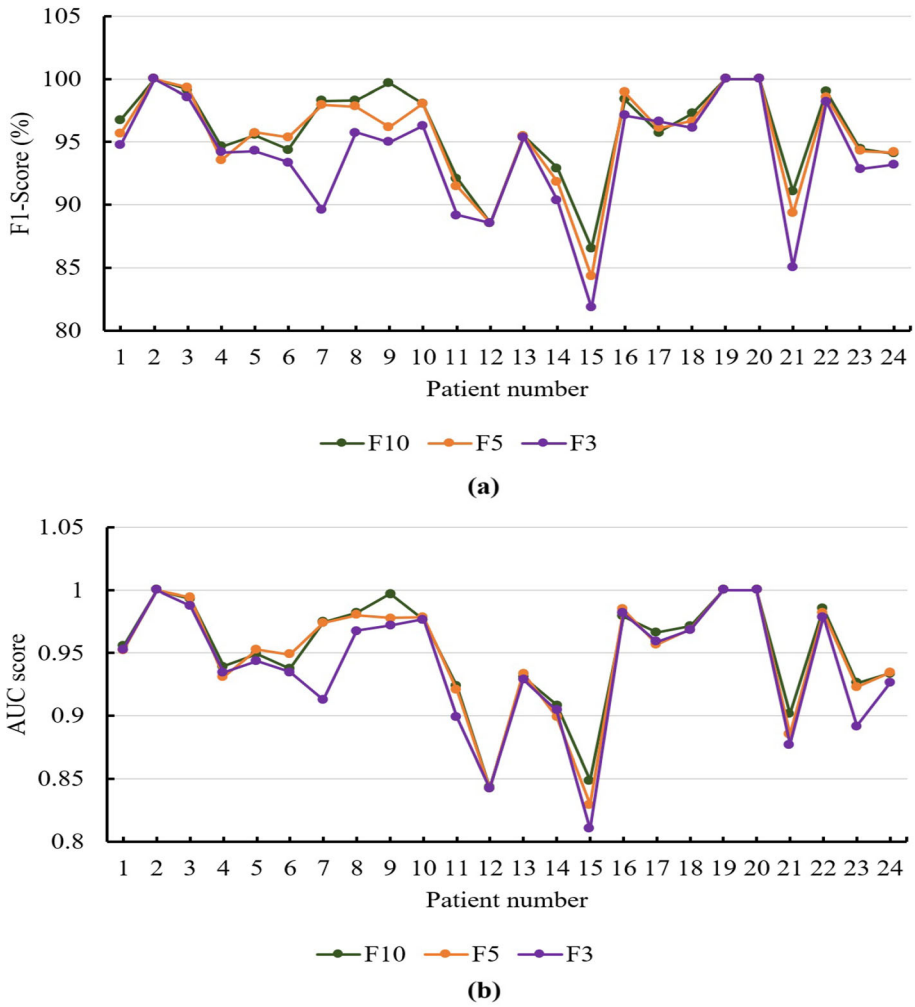

Fig. 8 Patient-specific feature selection with SMOTE applied to all patients from the CHB-MIT dataset using three feature sets: original 10 features (F10), top 5 features (F5), and top 3 features (F3). Results are presented for **a** F1-score and **b** AUC score

Table 7 Overall performance metrics obtained using patient-specific feature selection for the CHB-MIT dataset

Performance metrics	Number of features					
	Without SMOTE			With SMOTE		
	F10	F5	F3	F10	F5	F3
Avg. ACC	97.37	97.29	96.78	97.29	96.99	96.03
Avg. PRC	97.42	97.41	96.78	96.80	96.19	94.31
Avg. SEN	87.90	87.88	85.26	95.08	94.80	94.03
Avg. SPC	99.37	99.35	99.19	99.00	98.75	97.79
Avg. F1-SCR	92.14	92.13	90.28	95.85	95.38	94.01
Avg. AUC	0.9362	0.9359	0.9222	0.951	0.9479	0.9397

Avg.: Average, **ACC**: Accuracy, **PRC**: Precision, **SEN**: Sensitivity, **SPC**: Specificity, **F1-SCR**: F1-Score, **AUC**: Area under the ROC curve, **F10**: Ten features, **F5**: Top five features, **F3**: Top three features

However, since Shannon_ent alone (a rank 1 feature) did not yield satisfactory performance for certain patients in the Seina dataset, additional features from the next highest rank (rank 2) are incorporated to enhance the generalization, resulting in a robust feature set of four features for the patient-non-specific model.

A separate SA-RF model is trained for each patient in the CHB-MIT dataset using the three common features identified through our method and the findings are reported in Table 9. Similarly, for the Seina dataset, an individual SA-RF model is trained for each patient using the four

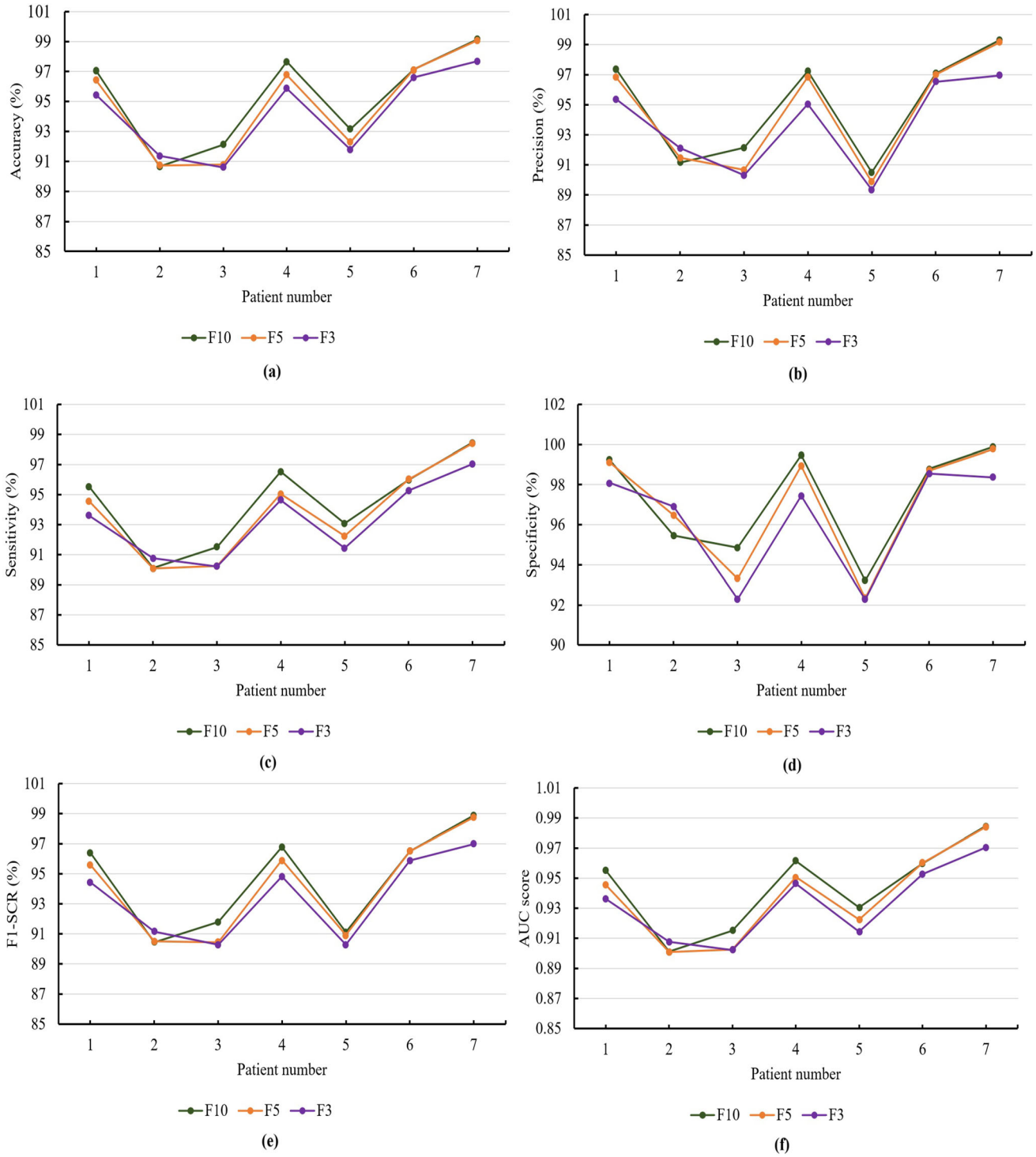

Fig. 9 Performance metrics obtained using patient-specific feature selection with SMOTE with the original 10 features (F10), top 5 selected features (F5), and top 3 selected features (F3) for the Seina dataset. The subfigures represent: **a** Accuracy, **b** Precision, **c** Sensitivity, **d** Specificity, **e** F1-Score, and **f** Area Under the Curve (AUC)

selected common features derived from our proposed approach and the results are presented in Table 10.

The performance of the SA-RF models trained using the selected common features is evaluated using standard performance metrics, both with and without the application of SMOTE, highlighting the effect of class imbalance handling on model performance across patients. Based on the performance metrics presented in Table 9 for the CHB-

Table 8 Overall performance metrics obtained using patient-specific feature selection for the Seina dataset

Performance metrics	Number of features					
	Without SMOTE			With SMOTE		
	F10	F5	F3	F10	F5	F3
Avg. ACC	95.07	94.60	94.05	95.27	94.74	94.19
Avg. PRC	94.86	94.48	93.52	94.97	94.55	93.67
Avg. SEN	93.53	93.20	92.39	94.46	93.81	93.29
Avg. SPC	97.10	96.89	96.27	97.27	96.95	96.28
Avg. F1-SCR	94.39	93.82	93.21	94.56	94.10	93.41
Avg. AUC	0.9372	0.9372	0.9247	0.9441	0.9381	0.9329

Avg.: Average, **ACC**: Accuracy, **PRC**: Precision, **SEN**: Sensitivity, **SPC**: Specificity, **F1-SCR**: F1-Score, **AUC**: Area under the ROC curve, **F10**: Ten features, **F5**: Top five features, **F3**: Top three features

MIT dataset, it is evident that the application of the selected common features: Shannon_ent, Std_dev, and Sample_ent in patient-non-specific SA-RF models yields strong results across patients. Without SMOTE, the average accuracy, precision, and F1-score obtained are 96.60%, 96.98%, and 99.25%, respectively, while the sensitivity and specificity achieved are 86.91% and 91.43%. The average AUC without SMOTE stands at 0.9308. With the application of SMOTE, a notable improvement is observed in sensitivity and overall class balance. The average sensitivity increases from 86.91 to 94.52%, and the AUC improves to 0.9452. Although the average accuracy and precision remain almost the same (96.58% and 95.19%, respectively), the application of SMOTE helps to reduce the disparity between sensitivity and specificity, ultimately enhancing the model's ability to detect seizures reliably. These results highlight the effectiveness of the selected common features and the beneficial impact of SMOTE on class imbalance handling in patient-non-specific seizure detection.

Based on the results shown in Table 10 for the Seina dataset, patient-non-specific models are evaluated using the selected common features: Shannon_ent, Std_dev, Sample_ent, and Kurtosis under both SMOTE and non-SMOTE settings.

Without applying SMOTE, the models achieved an average accuracy of 94.95%, precision of 95.01%, and F1-score of 94.24%. The sensitivity and specificity were 93.62% and 97.65%, respectively, with an AUC of 0.9362, indicating strong classification performance across all patients. Upon applying SMOTE, the performance metrics remained largely consistent, showing marginal improvements in sensitivity and AUC. The average sensitivity increased to 94.04%, and AUC slightly improved to 0.9400, while accuracy, precision, and F1-score stayed stable at 94.81%, 94.51%, and 94.28%, respectively.

These findings confirm that the performance of seizure detection using the reduced patient-non-specific feature set is robust, and that SMOTE further helps in addressing any class imbalance, particularly enhancing sensitivity without compromising overall accuracy.

The impact of SMOTE on the CHB-MIT and Seina datasets highlights the influence of class imbalance and seizure distribution on model performance. In the CHB-MIT dataset, applying SMOTE led to a significant improvement in sensitivity (from 86.91 to 94.52%), AUC (from 0.9308 to 0.9452), and other metrics, indicating that this dataset suffers from a more pronounced imbalance, likely due to shorter or infrequent seizure segments in some patients. This imbalance makes the model prone to bias towards the majority class, which SMOTE effectively counteracts by generating synthetic seizure samples. In contrast, the Seina dataset showed only marginal performance gains with SMOTE, suggesting it has more balanced and consistent seizure distributions across patients.

Comparison with other state-of-the-art work

To evaluate the effectiveness of our proposed SHAP-RELFR-based feature selection approach, we compared its performance with existing state-of-the-art methods reported in the literature. Furthermore, an ideal parameter configuration for the RF classifier has been identified using SA, which is essential for managing noisy and high-dimensional EEG data. Robust performance metrics across patients demonstrate the improvement in generalization and mitigation of overfitting resulting from this optimization stage. Table 11 presents a comparison of our findings with the state-of-the-art work reported by different researchers. Unlike prior studies that primarily relied on traditional approaches, our method has used explainable SHAP values for more robust and interpretable feature selection. Compared to traditional methods, the use of XAI-based SHAP not only enhances model performance but also offers greater transparency, making it

Table 9 Performance metrics obtained using the common features selected by the proposed SHAP-RELFR method for the patient-non-specific case on the CHB-MIT dataset, evaluated with and without the application of SMOTE

PID	ACC	PRC	SEN	SPC	F1-SCR	AUC
	Without SMOTE					
Patient 1	96.82	99.18	84.99	91.54	99.82	0.9241
Patient 2	100	100	100	100	100	1
Patient 3	99.46	97.73	98.77	98.25	99.59	0.9918
Patient 4	95.44	98.07	85.61	91.42	99.33	0.9247
Patient 5	97.29	95.72	88.47	91.96	99.16	0.9382
Patient 6	97.55	95.28	84.87	89.78	99.39	0.9213
Patient 7	98.88	98.22	93.94	96.03	99.71	0.9682
Patient 8	98.72	97.93	96.33	97.12	99.41	0.9786
Patient 9	99.76	99.10	99.32	99.21	99.84	0.9956
Patient 10	99.28	98	95.27	96.61	99.76	0.9752
Patient 11	88.44	90.20	71.81	79.96	96.31	0.8406
Patient 12	93.11	100	68.49	81.30	100	0.8424
Patient 13	97.9	99.68	87.39	93.13	99.94	0.9366
Patient 14	94.95	95.10	73.48	82.91	99.24	0.8636
Patient 15	87.28	94.70	73.15	82.54	97.14	0.8514
Patient 16	94.44	90.24	74.75	81.77	98.38	0.8657
Patient 17	94.75	94.08	83.58	88.52	98.32	0.9094
Patient 18	97.51	96.44	91.19	93.74	99.14	0.9516
Patient 19	100	100	100	100	100	1
Patient 20	100	100	100	100	100	1
Patient 21	93.8	95.49	71.91	82.04	99.17	0.8554
Patient 22	99.58	100	94.55	97.2	100	0.9727
Patient 23	97.17	97.55	82.06	89.14	99.66	0.9086
Patient 24	96.32	94.79	85.96	90.16	98.85	0.9241
Avg.	**96.60**	**96.98**	**86.91**	**91.43**	**99.25**	**0.9308**
	With SMOTE					
Patient 1	95.31	90.11	93.52	96.16	91.70	0.9352
Patient 2	100.00	100.00	100.00	100.00	100.00	1
Patient 3	99.51	99.38	99.38	99.67	99.38	0.9938
Patient 4	93.80	92.35	92.40	95.64	92.38	0.9240
Patient 5	95.36	94.04	94.19	96.73	94.12	0.9419
Patient 6	97.08	93.32	93.48	98.30	93.40	0.9348
Patient 7	97.82	96.52	96.25	98.74	96.38	0.9625
Patient 8	98.51	97.58	98.18	98.78	97.87	0.9818
Patient 9	99.86	99.64	99.83	99.88	99.73	0.9983
Patient 10	99.00	98.79	96.02	99.83	97.35	0.9602
Patient 11	92.21	90.66	91.80	92.94	91.19	0.9180
Patient 12	93.11	95.95	84.25	100.00	88.54	0.8425
Patient 13	97.28	98.37	92.92	100.00	95.36	0.9292
Patient 14	95.09	88.85	89.10	97.14	88.97	0.8910
Patient 15	87.95	88.38	84.14	95.63	85.74	0.8414
Patient 16	99.37	96.19	99.19	99.39	97.63	0.9919
Patient 17	97.07	96.68	96.62	97.88	96.65	0.9662
Patient 18	97.91	96.60	97.00	98.54	96.80	0.9700
Patient 19	100	100	100	100	100	1
Patient 20	100	100	100	100	100	1
Patient 21	89.54	82.64	87.20	91.06	84.58	0.8720
Patient 22	99.53	99.47	98.73	99.89	99.10	0.9873
Patient 23	96.73	96.12	90.11	99.35	92.82	0.9011
Patient 24	95.88	92.90	94.29	96.91	93.58	0.9429
Avg.	**96.58**	**95.19**	**94.52**	**98.02**	**94.72**	**0.9452**

PID: Patient ID, **Avg.**: Average, **ACC**: Accuracy, **PRC**: Precision, **SEN**: Sensitivity, **SPC**: Specificity, **F1-SCR**: F1-Score, **AUC**: AUC score

Table 10 Performance metrics obtained using the common features selected by the proposed SHAP-RELFR method for the patient-non-specific case on the Seina dataset, evaluated with and without the application of SMOTE

PID	ACC	PRC	SEN	SPC	F1-SCR	AUC
	Without SMOTE					
Patient 1	95.88	96.71	93.46	99.43	94.90	0.9346
Patient 2	91.53	92.12	90.99	96.48	91.35	0.9099
Patient 3	91.91	91.93	91.30	94.69	91.58	0.9130
Patient 4	96.82	97.04	95.00	99.11	95.96	0.9500
Patient 5	92.75	91.47	90.77	95.46	91.11	0.9077
Patient 6	97.06	96.99	95.94	98.71	96.44	0.9594
Patient 7	98.71	98.80	97.85	99.65	98.31	0.9785
Avg.	**94.95**	**95.01**	**93.62**	**97.65**	**94.24**	**0.9362**
	With SMOTE					
Patient 1	95.21	95.14	93.49	98.03	94.95	0.9329
Patient 2	91.61	92.30	91.83	96.92	91.42	0.9193
Patient 3	91.61	91.34	91.30	92.98	91.32	0.9130
Patient 4	96.65	96.52	95.07	98.63	95.96	0.9507
Patient 5	93.30	91.31	92.81	93.97	92.01	0.9281
Patient 6	96.60	96.13	95.93	97.90	95.98	0.9573
Patient 7	98.71	98.80	97.85	99.65	98.31	0.9785
Avg.	**94.81**	**94.51**	**94.04**	**96.87**	**94.28**	**0.9400**

PID: Patient ID, **Avg.**: Average, **ACC**: Accuracy, **PRC**: Precision, **SEN**: Sensitivity, **SPC**: Specificity, **F1-SCR**: F1-Score, **AUC**: AUC score

advantageous for clinical applications where understanding the contribution of each feature is crucial.

Compared to prior studies, our proposed approach demonstrates consistent and balanced performance across

Table 11 Comparison with other state-of-the-art works

Work	Performance metrics					
	ACC	PRC	SEN	SPC	F1-SCR	AUC
Hassan et al. (2022)	99.38	–	–	100	99.32	–
Behnam and Pourghassem (2017)	82.52	95.80	85.45	22.20	90.32	–
Orosco et al. (2016)	99.90	–	87.5	–	–	–
Chen et al. (2017)	92.30	92.80	91.71	92.89	–	–
Samiee et al. (2017)	–	–	71.60	99.20	98.80	0.854
	–	–	72.00	97.20	97.50	0.846
Yang et al. (2020)	98.28	–	98.93	97.64	–	–
	86.27	–	80.32	92.22	–	–
Jana et al. (2023)	93.50	–	93.19	93.90	93.66	0.9350
Poorani and Balasubramanie (2023)	94.83	99.43	90.18	99.43	94.50	–
Sadam and Nalini (2024)	94.48	94.10	94.90	–	–	–
Proposed work: CHB-MIT	96.99	96.19	94.80	98.75	95.38	0.9479
	96.58	95.19	94.52	98.02	94.72	0.9452
Proposed work: Seina	94.74	94.55	93.81	96.95	94.10	0.9381
	94.81	94.51	94.04	96.87	94.28	0.9400

ACC: Accuracy, **PRC**: Precision, **SEN**: Sensitivity, **SPC**: Specificity, **F1-SCR**: F1-score

multiple evaluation metrics. For instance, while the work (Hassan et al. 2022) reported a very high accuracy of 99.38% and good specificity of 100%, they did not provide sensitivity or AUC values, making it difficult to evaluate their model's seizure detection ability comprehensively. In contrast, our approach achieved an accuracy of 96.58%, a high sensitivity of 94.52%, and an AUC of 0.9452 on the CHB-MIT dataset, indicating strong and balanced classification performance. The study (Behnam and Pourghassem 2017) achieved 82.52% accuracy and 85.45% sensitivity, but their specificity dropped to 22.20%, suggesting a high rate of false alarms. Our model significantly outperforms this with 98.02% specificity, reducing misclassifications. The work (Orosco et al. 2016) reported very high accuracy of 99.90%, but again missed metrics such as specificity and AUC, making it difficult to evaluate the model's generalizability. The study (Chen et al. 2017) presented a balanced model with 92.30% accuracy and 91.71% sensitivity, yet our proposed method outperforms it across all metrics, particularly with a higher AUC of 0.9452. The implementation (Samiee et al. 2017) had high F1-scores, but their low sensitivity (71.60%−72.00%) shows that their model missed many seizure events. The methodology (Yang et al. 2020) reported an outstanding sensitivity of 98.93%, accuracy of 98.26%, and specificity of 97.64%; even our method maintains stable and high performance across datasets.

Among recent studies, the work (Jana et al. 2023) achieved 93.60% F1-score but an accuracy of 93.50%, while (Poorani and Balasubramanie 2023) reported a high accuracy of 94.83% and sensitivity of 93.99%, but still slightly behind our CHB-MIT performance. The implementation (Sadam and Nalini 2024) showed competitive performance with 94.48% accuracy and 94.90% sensitivity; however, the accuracy is slightly lower compared to our proposed model, which has achieved up to 96.99% on the CHB-MIT dataset. However, our model consistently outperforms in AUC and generalizes better across datasets.

This proposed work takes advantage of the ability to choose from a flexible number of features, providing a trade-off between the necessary computational power and the classifier's performance. Utilizing just 3 or 4 features for the CHB-MIT or Seina datasets reduces the computational resources needed significantly, without compromising classifier performance. In contrast, Hassan et al. (2022) has employed 9 features after the feature selection stage, whereas (Yang et al. 2020) has utilized 30 features.

This proposed methodology shows significant gains in patient-specific and patient-non-specific approaches of feature selection compared to existing seizure detection techniques. Because seizure occurrences are complicated and unique, traditional methods, which frequently rely on fixed feature sets and less advanced optimization techniques, tend to perform poorly. The comparative analysis highlights the proposed method's contributions and developments, emphasizing its potential as a useful tool for seizure detection.

Overall, while several prior studies have achieved strong performance in specific metrics, many of them lack consistency across all key parameters such as sensitivity, specificity, and AUC. Our proposed SHAP-based feature selection and SA-RF method demonstrates a more

balanced and robust performance across both the CHB-MIT and Seina datasets, achieving high accuracy, sensitivity, and specificity with excellent AUC values. By integrating explainable AI for reliable feature selection, our approach not only enhances seizure detection but also ensures better generalization and interpretability, making it a more reliable and effective solution compared to traditional and recent methods.

Discussion

The findings of this proposed work show that the Explainable AI (XAI) framework, incorporated with SMOTE and the simulated annealing optimized RF classifier, greatly enhances seizure detection performance. The SHAP value-based patient-specific feature selection has shown promising results by effectively identifying the most influential features for each individual, leading to improved model performance and enhanced interpretability in seizure detection. The contribution of each feature to model prediction is more effectively examined using the SHAP summary plot and SHAP bar graph. According to this proposed work, each patient has a different feature ranking as shown in Tables 3 and 4, revealing that different features have diverse roles in seizure detection. This diversity in features highlights the necessity for customized models, which emphasize the variation in seizure manifestations among patients. For nearly all patients in the CHB-MIT dataset and Seina dataset, Shannon_ent is found to have the greatest impact on model prediction. Thus, this proposed approach will assist in choosing the top k features for the seizure detection model. The essential predictive capability could be maintained even after the model is reduced to 5 features, as demonstrated in Tables 7 and 8, despite the model becoming less complex and requiring fewer computing resources. Because of this balance, the model with 5 features obtained using a patient-specific feature selection method is a desirable choice for practical applications where computational performance is an important consideration.

This research work has demonstrated a systematic and reliable procedure to identify the best common features that can be utilized across models of each patient. The proposed SHAP-RELFR patient-non-specific feature selection method has obtained Shannon_ent, Std_dev, and Sample_ent features as the most effective feature set that can be used to train models of all patients of the CHB-MIT dataset. Similarly, Shannon_ent, Std_dev, Sample_ent, and Kurtosis are obtained as a common feature set that can be used for training the model of all patients in the Seina dataset. The proposed novel SHAP-RELFR method for patient-non-specific feature selection has been evaluated by estimating the performance metrics of each patient. This suggests that, irrespective of patient-specific characteristics, three or four features have a generalizable predictive power for seizure detection of patients from the CHB-MIT or Seina datasets. It can function as a baseline model that can be refined further on patient-specific data, offering a versatile framework for seizure detection in a diverse clinical setting.

The RF model, validated using 5-fold cross-validation with SMOTE, demonstrates robustness across multiple data splits, thereby minimizing the risk of overfitting and ensuring better generalization to unseen data. Using the CHB-MIT dataset, the patient-specific feature selection method yields an impressive key performance metric as illustrated in Table 7. An average value of accuracy 96.99%, precision of 96.19%, sensitivity of 94.80%, specificity of 98.75%, F1-score of 95.38%, and AUC of 0.9479. As shown in Table 9, the patient-non-specific approach also demonstrates strong performance, yielding results that are closely comparable to those of the patient-specific feature selection method. For the Seina dataset, as depicted in Table 8, an average value of accuracy 94.74%, precision of 94.55%, sensitivity of 93.81%, specificity of 96.95%, F1-score of 94.10%, and AUC of 0.9381 are obtained for the patient-specific feature selection. Whereas, the average value of accuracy, precision, sensitivity, specificity, F1-score, and AUC obtained by patient-non-specific features are 94.81%, 94.51%, 94.04%, 96.87%, 94.28%, and 0.9400, respectively.

By optimizing model performance and lowering computational complexity, the use of SHAP values for feature reduction in seizure detection not only improves clinical results but also increases the interpretability and reliability of machine learning models through Explainable AI (XAI) (Frasca et al. 2024). Healthcare practitioners can gain important insights into the mechanisms behind epilepsy and open the door for customized, data-driven approaches to patient care. SA helps avoid local minima, ensuring optimal feature selection by efficiently searching through large feature spaces. The SA optimization method skillfully strikes a balance between exploring and exploiting the hyperparameter space and optimizing the model for better performance.

This proposed work demonstrates strong performance and interpretability; however, real-time implementation aspects such as latency, computational load, and hardware feasibility are not explored. Since the methods employed in this work, such as DWT-based signal decomposition, feature extraction, SHAP-based interpretability, and RF classification, are relatively lightweight, they have the potential for real-time use. Future investigations may involve analyzing the execution time, evaluating processing delays, and testing on resource-constrained platforms to confirm the system's suitability for clinical or wearable deployment.

Conclusion

The main contribution of the proposed methodology is to present a novel framework that provides an enhanced method for seizure detection using multichannel EEG signals by integrating DWT, statistical and entropy-based features, SHAP-based feature selection, SMOTE, and SA-RF classifier. SHAP-based patient-specific and patient-non-specific feature selection methods offer unique advantages in developing machine learning models for seizure detection. By tailoring feature selection for each patient, the framework improves the model's capacity to customize treatments and predictions. It simultaneously integrates feature selection that is not specific to a patient to find features that are relevant to all patients using a novel SHAP-RELFR method. SA balances exploring new feature subsets with focusing on promising ones, leading to better solutions. Furthermore, the application of SMOTE addressed the issue of class imbalance, particularly improving sensitivity in the minority seizure class. Both patient-specific and patient-non-specific approaches benefited from SMOTE, showing improved sensitivity without compromising specificity or overall accuracy. The proposed methodology is rigorously evaluated using two benchmark datasets, CHB-MIT and Seina. The performance metrics obtained using both approaches remain consistently high even after reducing the number of features, indicating that the model performs robustly and effectively. This consistency in performance metrics indicates that the feature selection process effectively identifies the most relevant features.

In addition to improving transparency, SHAP values offer a strong framework for analyzing feature relevance, enabling us to keep the features that have the biggest impact on the model's predictive capability. This proposed low-cost and efficient seizure detection system using SHAP value will aid in refining the feature engineering, improving the model interpretability, and assisting clinicians in optimizing clinical decision-making. Future developments may include automated parameter tuning, hybrid optimization, and real-time implementation on resource-constrained platforms.

Funding The authors declare that no funds, grants, or other support were received for this work.

Data Availability The data used in this work is obtained from publicly available sources: https://physionet.org/content/chbmit/1.0.0/ and https://physionet.org/content/siena-scalp-eeg/1.0.0/.

Declarations

Conflict of interest The authors have no relevant financial or non-financial interests to disclose.

Ethical approval and informed consent Ethical approval and informed consent are not required for this work, as it utilized publicly available datasets. The datasets used in this research were obtained from physionet.org.

References

Acharya UR, Hagiwara Y, Koh JEW, Shu Lih O, Tan JH, Adam M, Tan RS (2018) Entropies for automated detection of coronary artery disease using ECG signals: a review. Biocybern Biomed Eng 38(2):373–384

Ahmad I, Yao C, Li L, Chen Y, Liu Z, Ullah I, Shabaz M, Wang X, Huang K, Li G et al (2024) An efficient feature selection and explainable classification method for EEG-based epileptic seizure detection. J Inf Secur Appl 80:103654

Amengual-Gual M, Fernández IS, Loddenkemper T (2019) Patterns of epileptic seizure occurrence. Brain Res 1703:3–12

Bandt C, Pompe B (2002) Permutation entropy: a natural complexity measure for time series. Phys Rev Lett 88(17):174102

Bashir N, Narejo S, Naz B, Ismail F, Anjum MR, Butt A, Anwar S, Prasad R (2023) A machine learning framework for major depressive disorder (MDD) detection using non-invasive EEG signals. Wirel Pers Commun 1–23

Behnam M, Pourghassem H (2015) Periodogram pattern feature-based seizure detection algorithm using optimized hybrid model of MLP and ant colony. In 2015 23rd Iranian conference on electrical engineering. IEEE, pp 32–37

Behnam M, Pourghassem H (2017) Spectral correlation power-based seizure detection using statistical multi-level dimensionality reduction and PSO-PNN optimization algorithm. IETE J Res 63(5):736–753

Chandran KS, Perumalsamy M (2018) EEG based strategies for human gustation classification using spartan-6 FPGA. Wirel Pers Commun 103(4):3041–3053

Chawla NV, Bowyer KW, Hall LO, Kegelmeyer WP (2002) Smote: synthetic minority over-sampling technique. J Artif Intell Res 16:321–357

Chen D, Wan S, Xiang J, Bao FS (2017) A high-performance seizure detection algorithm based on discrete wavelet transform (DWT) and EEG. PLoS ONE 12(3):e0173138

Cunningham P (2008) Dimension reduction. In: Machine learning techniques for multimedia: case studies on organization and retrieval. Springer, pp 91–112

Detti P (2020) Siena scalp EEG database (version 1.0.0)

Detti P, Vatti G, Zabalo Manrique de Lara G (2020) EEG synchronization analysis for seizure prediction: a study on data of noninvasive recordings. Processes 8(7):846

Dokare I, Gupta S (2025) Optimized seizure detection leveraging band-specific insights from limited EEG channels. Health Inf Sci Syst 13(1):30

Faust O, Acharya RU, Allen AR, Lin CM (2008) Analysis of EEG signals during epileptic and alcoholic states using AR modeling techniques. IRBM 29(1):44–52

Fernández A, Garcia S, Herrera F, Chawla NV (2018) Smote for learning from imbalanced data: progress and challenges, marking the 15-year anniversary. J Artif Intell Res 61:863–905

Frasca M, La Torre D, Pravettoni G, Cutica I (2024) Explainable and interpretable artificial intelligence in medicine: a systematic bibliometric review. Discover Artif Intell 4(1):15

Gandomi AH, Yang X-S, Talatahari S, Alavi AH (2013) Metaheuristic algorithms in modeling and optimization. In: Metaheuristic applications in structures and infrastructures, vol 1, pp 1–24

Goldberger Ary L, Amaral Luis AN, Leon G, Hausdorff Jeffrey M, Ivanov Plamen Ch, Mark Roger G, Mietus Joseph E, Moody

George B, Chung-Kang P, Eugene SH (2000) Physiobank, physiotoolkit, and physionet: components of a new research resource for complex physiologic signals. Circulation 101(23):e215–e220

Gotman J, Gloor P (1976) Automatic recognition and quantification of interictal epileptic activity in the human scalp EEG. Electroencephalogr Clin Neurophysiol 41(5):513–529

Guo Y, Zhang Y, Mursalin M, Xu W, Lo B (2018) Automated epileptic seizure detection by analyzing wearable EEG signals using extended correlation-based feature selection. In: 2018 IEEE 15th international conference on wearable and implantable body sensor networks (BSN). IEEE, pp 66–69

Gupta V, Kanungo A, Kumar P, Kumar N, Choubey C (2023) A design of bat-based optimized deep learning model for EEG signal analysis. Multimedia Tools Appl 82(29):45367–45387

Gupta V, Kanungo A, Saxena NK, Kumar P, Kumar P (2023) An adaptive optimized schizophrenia electroencephalogram disease prediction framework. Wirel Pers Commun 130(2):1191–1213

Gupta V, Mittal M, Mittal V, Diwania S, Singh R, Gupta V (2024) A firefly based deep belief signal specification based novel hybrid technique for EEG signal analysis. IETE J Res 70(5):5263–5269

Hasan MM, Hossain MM, Mia S, Ahammad MS, Rahman MM (2022) A combined approach of non-subsampled contourlet transform and convolutional neural network to detect gastrointestinal polyp. Multimedia Tools Appl 81(7):9949–9968

Hasan MM, Hossain MM, Rahman MM, Azad A, Alyami SA, Moni MA (2023) FP-CNN: fuzzy pooling-based convolutional neural network for lung ultrasound image classification with explainable ai. Comput Biol Med 165:107407

Hassan KM, Islam MR, Nguyen TT, Molla MKI (2022) Epileptic seizure detection in EEG using mutual information-based best individual feature selection. Expert Syst Appl 193:116414

Hossain MM, Hasan MM, Rahim MA, Rahman MM, Yousuf MA, Al-Ashhab S, Akhdar HF, Alyami SA, Azad A, Moni MA (2022) Particle swarm optimized fuzzy CNN with quantitative feature fusion for ultrasound image quality identification. IEEE J Transl Eng Health Med 10:1–12

Hossain MM, Walid MA, Galib SS, Azad MM, Rahman W, Shafi AS, Rahman MM (2024) Covid-19 detection from chest ct images using optimized deep features and ensemble classification. Syst Soft Comput 6:200077

Jana GC, Swami K, Agrawal A (2023) Capsule neural network based approach for subject specific and cross-subjects seizure detection from eeg signals. Multimedia Tools Appl 82(23):35221–35252

Khare SK, Bajaj V (2022) Optimized tunable q wavelet transform based drowsiness detection from electroencephalogram signals. Irbm 43(1):13–21

Kirkpatrick S, Daniel Gelatt Jr C, Vecchi MP (1983) Optimization by simulated annealing. Science 220(4598):671–680

Kondo M, Bezemer C-P, Kamei Y, Hassan AE, Mizuno O (2019) The impact of feature reduction techniques on defect prediction models. Empir Softw Eng 24:1925–1963

Kundu S, Ari S (2022) Brain-computer interface speller system for alternative communication: a review. IRBM 43(4):317–324

Lundberg Scott M, Lee S-I (2017) A unified approach to interpreting model predictions. In: Advances in neural information processing systems, vol 30

Ma P, Dong C, Lin R, Ma S, Liu H, Lei D, Chen X (2023) Effect of local network characteristics on the performance of the SSVEP brain-computer interface. IRBM 44(4):100781

Macready WG, Wolpert DH (1996) What makes an optimization problem hand? Complexity 1(5):40–46

Malan NS, Sharma S (2022) Motor imagery EEG spectral-spatial feature optimization using dual-tree complex wavelet and neighbourhood component analysis. IRBM 43(3):198–209

Mostafiz R, Uddin MS, Jabin I, Hossain MM, Rahman MM (2022) Automatic brain tumor detection from MRI using curvelet transform and neural features. IJACI 13(1):1–18

Mursalin Md, Zhang Y, Chen Y, Chawla NV (2017) Automated epileptic seizure detection using improved correlation-based feature selection with random forest classifier. Neurocomputing 241:204–214

Narin A (2022) Detection of focal and non-focal epileptic seizure using continuous wavelet transform-based scalogram images and pre-trained deep neural networks. Irbm 43(1):22–31

Omidvar M, Zahedi A, Bakhshi H (2021) EEG signal processing for epilepsy seizure detection using 5-level db4 discrete wavelet transform, ga-based feature selection and ann/svm classifiers. J Ambient Intell Humaniz Comput 12(11):10395–10403

Orosco L, Correa AG, Diez P, Laciar E (2016) Patient non-specific algorithm for seizures detection in scalp EEG. Comput Biol Med 71:128–134

Pais-Ribeiro J, Meneses RF (2011) Positive psychosocial variables and outcome variables in persons with epilepsy. Management of epilepsy-research results and treatment. CCBY-NC-SA 3:171–194

Peng G, Nourani M, Harvey J, Dave H (2021) Personalized EEG feature selection for low-complexity seizure monitoring. Int J Neural Syst 31(08):2150018

PhysioNet (2010) Chb-mit scalp eeg database. https://physionet.org/content/chbmit/1.0.0/, June. Accessed on 01 Apr 2022

PhysioNet (2020) Siena scalp EEG database. https://physionet.org/content/siena-scalp-eeg/1.0.0/. Accessed on 12 Nov 2024

Polat K, Nour M (2020) Epileptic seizure detection based on new hybrid models with electroencephalogram signals. Irbm 41(6):331–353

Poorani S, Balasubramanie P (2023) Deep learning based epileptic seizure detection with EEG data. Int J Syst Assurance Eng Manag pp 1–10

Rampil IJ (1998) A primer for EEG signal processing in anesthesia. J Am Soc Anesthesiologists 89(4):980–1002

Richman JS, Moorman JR (2000) Physiological time-series analysis using approximate entropy and sample entropy. Am J Physiol-Heart Circulatory Physiol 278(6):H2039–H2049

Sadam SSP, Nalini NJ (2024) Epileptic seizure detection using scalogram-based hybrid CNN model on EEG signals. SIViP 18(2):1577–1588

Samiee K, Kovács P, Gabbouj M (2017) Epileptic seizure detection in long-term EEG records using sparse rational decomposition and local Gabor binary patterns feature extraction. Knowl-Based Syst 118:228–240

Sánchez-Hernández SE, Salido-Ruiz RA, Torres-Ramos S, Román-Godínez I (2022) Evaluation of feature selection methods for classification of epileptic seizure EEG signals. Sensors 22(8):3066

Sanei S, Chambers JA (2013) EEG signal processing. Wiley, Hoboken

Sanei S, Chambers JA (2021) EEG signal processing and machine learning. Wiley, Hoboken

Shapley LS (1953) Additive and non-additive set functions. Princeton University, Princeton

Shoeb A, Edwards H, Connolly J, Blaise Bourgeois S, Treves T, Guttag J (2004) Patient-specific seizure onset detection. Epilepsy Behavior 5(4):483–498

Shoeb AH, Guttag JV (2010) Application of machine learning to epileptic seizure detection. In: Proceedings of the 27th international conference on machine learning (ICML-10), pp 975–982

Shoeb AH (2009) Application of machine learning to epileptic seizure onset detection and treatment. PhD thesis, Massachusetts Institute of Technology

Siuly S, Li Y, Zhang Y (2016) EEG signal analysis and classification. IEEE Trans Neural Syst Rehabilit Eng 11:141–144
Strang G, Nguyen T (1996) Wavelets and filter banks. SIAM, Philadelphia
Suman B, Kumar P (2006) A survey of simulated annealing as a tool for single and multiobjective optimization. J Oper Res Soc 57:1143–1160
Sundaram M, Sadler RM, Young GB, Pillay N (1999) Eeg in epilepsy: current perspectives. Can J Neurol Sci 26(4):255–262
Tallón-Ballesteros A, Chen C (2020) Explainable AI: using shapley value to explain complex anomaly detection ml-based systems. Mach Learn Artif Intell 332:152
Van Laarhoven PJ, Aarts EH, van Laarhoven PJ, Aarts EH (1987) Simulated annealing. Springer, Berlin
Wang N, Lyu MR (2014) Extracting and selecting distinctive EEG features for efficient epileptic seizure prediction. IEEE J Biomed Health Inform 19(5):1648–1659
WHO (2022) Epilepsy. https://www.who.int/news-room/fact-sheets/detail/epilepsy, February
Wijayanto I, Hartanto R, Nugroho HA (2021) Wrapper subset feature selection for optimal feature selection in epileptic seizure signal classification. In: Proceedings of the 1st international conference on electronics, biomedical engineering, and health informatics: ICEBEHI 2020, 8–9 Oct, Surabaya, Indonesia. Springer, pp 567–577
Xiong Y, Dong F, Duanpo W, Jiang L, Liu J, Li B (2022) Seizure detection based on improved genetic algorithm optimized multilayer network. IEEE Access 10:81343–81354
Yadav SK, Tiwari PK, Tripathi A, Sharma UK, Dixit P, Dutt A, Prakash S, Shukla NK (2023) Comparative analysis of signal processing techniques for mental state recognition in brain-computer interfaces (BCI). Wirel Pers Commun 131(3):1569–1592
Yalcin N, Tezel G, Karakuzu C (2015) Epilepsy diagnosis using artificial neural network learned by PSO. Turk J Electr Eng Comput Sci 23(2):421–432
Yang S, Li B, Zhang Y, Duan M, Liu S, Zhang Y, Feng X, Tan R, Huang L, Zhou F (2020) Selection of features for patient-independent detection of seizure events using scalp EEG signals. Comput Biol Med 119:103671
Yang X-S (2010) Engineering optimization: an introduction with metaheuristic applications. Wiley, Hoboken